ISSN 1819-7140, Russian Journal of Pacific Geology, 2016, Vol. 10, No. 3, pp. 168–188. © Pleiades Publishing, Ltd., 2016.
Original Russian Text © V.A. Guryanov, A.N. Didenko, A.Yu. Peskov, G.V. Roganov, V.A. Dymovich, 2016, published in Tikhookeanskaya Geologiya, 2016, Vol. 35, No. 3, pp. 23–44.

# Early Precambrian Granitoids of the Batomga Inlier of the Southeastern Siberian Platform Basement: Age and Geodynamic Formation Settings

**V. A. Guryanov[a], A. N. Didenko[a, b], A. Yu. Peskov[a], G. V. Roganov[c], and V. A. Dymovich[c]**

[a] *Kosygin Institute of Tectonics and Geophysics (ITiG DVO RAN), Far East Branch, Russian Academy of Sciences, ul. Kim Yu Chena 65, Khabarovsk, 680000 Russia*

*e-mail: guryanov_v@mail.ru*

[b] *Geological Institute, Russian Academy of Sciences, Pyzhevskii per. 7, Moscow, 119017 Russia*

[c] *Center of Regional Geological Investigations, Open Joint-Stock Company Dal'geofizika, ul. L. Tolstogo 8, Khabarovsk, 680000 Russia*

Received April 30, 2015

**Abstract**—New data on the age, composition, sources, and formation conditions of the Early Precambrian granitoids of the Batomga inlier of the southeastern Siberian Platform basement are discussed. Geochronological SRHIMP II U–Pb study of the zircons reveals that the calc-alkaline granitoids of the Khoyunda Complex are 2056–2057 Ma in age and their formation was related to the Early Proterozoic stage in the development of the Batomga granite–greenstone domain. It is established that the primary melts for these rocks formed in subduction settings through melting of the depleted mantle source with some contribution of ancient crustal material. In terms of temperature, partial melting followed by crystallization of the granitoids under peak metamorphic conditions corresponds to the transition between amphibolite and granulite facies at elevated pressure; high temperature and high-grade metamorphism are subduction-related phenomena reflected in the back-arc settings of the active continental margin. The protoliths of calc-alkaline metavolcanics of the Batomga Group are found to be chronologically and compositionally analogous to the subduction granitoids of the Khoyunda and Dzhagdakan complexes; i.e., these granitoids are coeval with the Batomga island arc. The lower age limit of the Batomga Group is estimated at 2.2 Ga and its upper age limit is defined by the age of the intruded Khoyunda granitoids. The formation of the rocks of the Batomga Group and associated granitoids of the Khoyunda and Dzhagdakan complexes reflects the formation of the continental crust at the Early Paleoproterozoic stage of the evolution of the Batomga lithosphere block (2.2–2.0 Ga ago).

*Keywords*: Paleoproterozoic, Khoyunda Complex, Batomga Group, subduction, zircon, Batomga block, Siberian Platform

**DOI:** 10.1134/S1819714016030039

## INTRODUCTION

In the present-day structure of the southeastern Siberian Platform, the Batomga megablock represents an inlier of the Early Precambrian basement bounded by a system of graben-shaped troughs: aulacogens and depressions [2, 4, 13, 44]. This nearly inaccessible area of the Aldan–Stanovoi Shield is insufficiently known with respect to the evolution of magmatism, metamorphism, and geodynamics. Therefore, many aspects of its stratigraphy and magmatism are controversial. Many researchers have studied the Batomga terrane (block, inlier) [10, 16–21, 26–29, 34, 35]. Among them, A.P. Smelov contributed greatly to the study of this object [32–34, 50]. The principles and methods of the terrane analysis, tectonic zoning, interpretation of the basement structure, and paleogeodynamic reconstructions of the North Asian craton developed by this researcher and his colleagues are used in many works dedicated to the Early Precambrian evolution of the region. Smelov and V.F. Timofeev considered "The thorough study of the kinematics of the fractures which bound the terranes and form both at the stage of collision (accretion) and subsequent collapse of an orogen" as being "an important aspect" and one of the principal directions in the study of the ensemble of Early Precambrian terranes of Siberia. Such an approach allowed them to be among the first to conclude that "The period of 1900–1600 Ma ago was marked by the left-lateral displacement of the southern terranes of the North Asian and Sino-Korean cratons relative to northern terranes of the North Asian Craton ... *the process was likely related to the continuing formation of the Pangea supercontinent* ..." [33]. In his works, Smelov paid particular attention to the Batomga terrane, which is also an object of our

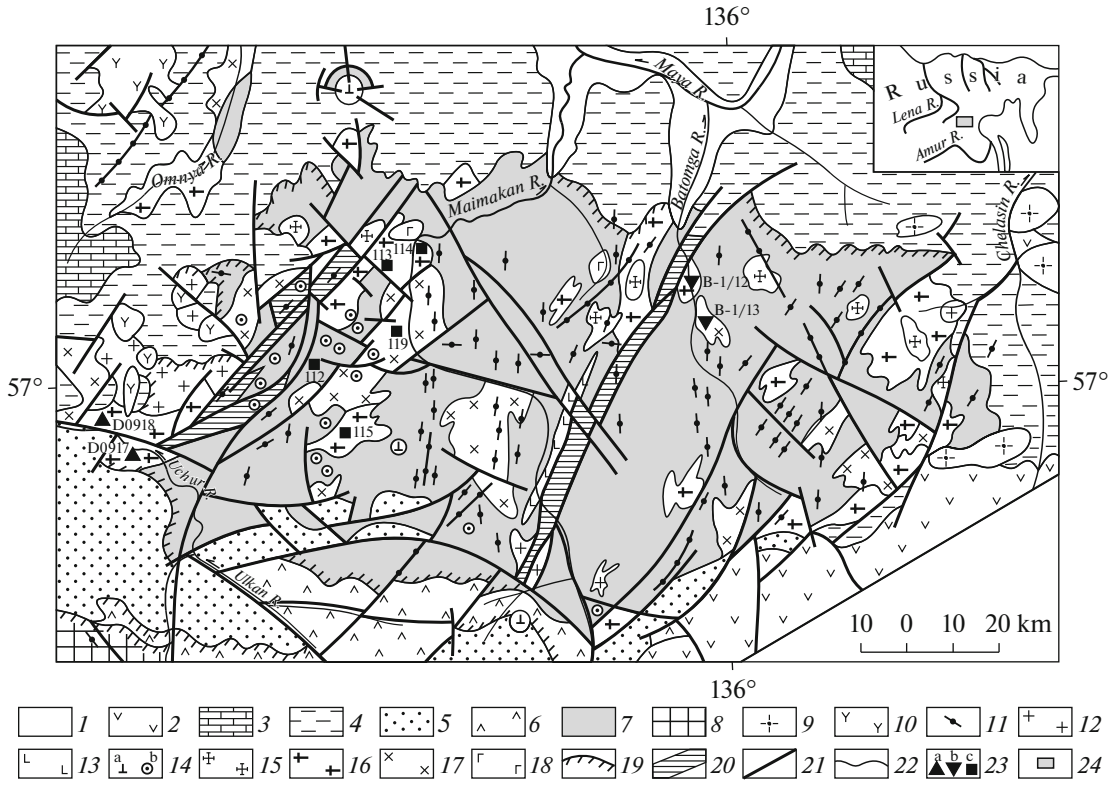





**Fig. 1.** Schematic geological structure of the Batomga inlier of the basement (after [11], modified).

(*1*) Neogene–Quaternary unconsolidated sediments; (*2*) Cretaceous volcanics of the Fore-Dzhugdzhur zone; (*3–5*) platform cover: (*3*) Upper Neoproterozoic–Lower Cambrian; (*4*) Upper Mesoproterozoic–Lower Neoproterozoic, undivided (Aimchan, Kerpyl, Lakhanda, and Ui groups); (*5*) Lower Riphean; (*6*) Upper Paleoproterozoic Ulkan Group; (*7*, *8*) crystalline basement: (*7*) Batomga Group (Utukachan, Odola, and Maimakan formations), (*8*) Lurikan Formation; (*9*) Late Cretaceous granites; (*10*) Early Cretaceous granitoids; (*11*) dikes and dike swarms of gabbrodolerites, dolerites, and gabbro (PR–PZ); (*12*, *13*) Late Paleoproterozoic granites (*12*) and gabbrodolerites (*13*); (*14*) Paleoproterozoic dunites, clinopyroxenites, and gabbro of the Konder Complex: (a) intrusions of the central type, (b) stocks and dikes (out of scale); (*15–18*) Early Paleoproterozoic leucogranites of the Tygymat (*15*), plagiogranites of the Khoyunda (*16*), quartz diorites of the Dzhagdakan (*17*), and metagabbroids of the Utukachan (*18*) complexes; (*19*) Proterozoic weathering crusts; (*20*) Chumican Complex of blastomilonites; (*21*) tectonic fractures; (*22*) geological boundaries; (*23*) sampling sites for isotopic–geochronological investigations: (a) this work U–Pb, zircon, SHRIMP II [14]; (b) Mishkin et al. (U–Pb, zircon, isochron) [26]; (c) Chepygin et al., 1998 (Rb–Sr, isochron [11]); (*24*) location of the Batomga inlier (inset).

geochronological and geodynamic studies in this work.

The Batomga inlier of the basement is a principal structural element of the synonymous megablock in the southeastern Siberian Platform. It is composed of supracrustal and plutonic rocks of Archean–Paleoproterozoic age and belongs to the Paleoproterozoic folded region [20, 21, 27]. Its constituting rock complexes metamorphosed from greenschist to amphibolite facies are characterized by a diverse composition [11, 20, 21, 27, 38]. A significant part of the Batomga inlier is occupied by outcrops of compositionally variable granitoids, which are attributed to Early Archean complexes in recent geological maps and correlation scales [9, 11, 17, 24, 31]. However, recent geochronological investigations have revealed that they are Early Paleoproterozoic in age (late Early Karelian) [13, 26]. These data make the dating and comprehensive study both of the magmatic and host metamorphic complexes constituting this inlier of the basement extremely crucial.

The investigations included the sampling of the Early Precambrian granitoids of the Batomga inlier, their geochemical analysis, and U–Pb isotopic dating (SHRIMP II) of zircons from these samples. The results are discussed below. The Khoyunda massif of "typical Early Archean" granitoids, which serve as a petrotype for the synonymous complex located on the left and right sides of the Khoyunda River, was selected as a study object (Fig. 1). A batch of granitoid samples from different massifs stored as standard collections in the Federal State Geological Department Khabarovskgeologiya was also used for geochemical investigations and results of silicate analyses of these samples were taken from the database to Sheet O-53 of the State geological map [11].

## GEOLOGICAL SITUATION

The Batomga inlier of the Early Precambrian basement represents a large (200 × 85 km) tectonic block extending in the sublatitudinal direction from the Uchur River in the west to the Chelasin River in the east (Fig. 1). Medium-scale geological surveying and special investigations have made it possible to develop the stratigraphic model for the Lower Precambrian sequences [18, 20], which are largely composed of rocks metamorphosed to the amphibolite facies [6–8, 20]. The metamorphic rocks are united into three formations (from the base upward): Utukachan, Odola, and Maimakan. In accordance with the Lower Precambrian stratigraphic scale accepted at that time, they were dated as Early Proterozoic. The results of the first K–Ar geochronological studies of the granitoids and dioritoids associated with the metamorphites of the above-mentioned formations give reason to assume that they were formed in the period of 2318–1906 Ma ago (Table 1) [6–8]. These data were accepted as a basis for the development of the first stratigraphic scales and for defining the magmatism stages for the Batomga block [20, 27]. The Utukachan Formation, 2000 m thick, is represented by a homogeneous sequence of biotite and biotite–hornblende plagiogneisses and crystalline schists with intercalations and lenses of amphibolites, hornblende–clinopyroxene, biotite–garnet, sillimanite gneisses, and marbles. The Odola Formation, 2500 m thick, is dominated by hornblende, clinopyroxene–hornblende plagiogneisses, crystalline schists, and amphibolites. The Maimakan Formation, 2000 m thick, is largely composed of biotite–hornblende and biotite plagiogneisses and crystalline schists with intercalations of marbles, amphibolites, and diopside plagiogneisses. All three formations are united into the Batomga Group [20]. The latter includes metagabbro, metapyroxenite, gabbro–amphibolite, and ortho-amphibolite bodies of the Utukachan Complex, which are deformed together with the host metamorphites into folds and migmatized [23]. These metabasites form relatively rare substratiform linear bodies, which are mostly emplaced into the metamorphic rocks of the Utukachan Formation [7, 11]. Their contacts with the host rocks are distinct, without exocontact alterations. Previously, they were described by some researchers as elements of formations being interpreted as initially volcanic or sedimentary in origin [4, 16, 18, 26, 28]. Subsequently, the stratigraphic scale of the area under consideration was repeatedly revised, usually in favor of older ages of the metamorphic sequences. For example, when compiling the map of metamorphism for southeastern East Siberia, Neelov et al. [28] subdivided the bedded crystalline sequences of the Batomga Group into three different age complexes: Early Archean Omnya, Late Archean Batomga, and Early Proterozoic Chumikan. They were correlated with the Zverevo, Stanovoi (Olekma), and Olonda groups in the western areas of the Aldan–Stanovoi shield [28]. According to the latter authors, each complex is characterized by a specific structure of sections, as well as by particular igneous rocks, metamorphism, and metallogeny. In opinion of [28], the rocks of the Omnya Complex experienced metamorphic alteration to the extent of the granulite facies being represented by two-pyroxene and hypersthene crystalline schists and plagiogneisses, biotite–garnet and sillimanite schists, quartzites, amphibolites, and calciphires. The rocks of the amphibolite facies were attributed to the Batomga Complex.

Subsequently, in connection with the revision of the geological age of the Stanovoi Complex and coeval rocks of the Aldan–Stanovoi Shield in favor of its older values, the Batomga Group and associated migmatites of the Utukachan, Dzhagdakan, Khoyunda, Levyi Chumikan, and Tygymat complexes were dated to the Early Archean and the Chumikan Group was attributed to the Late Archean [16, 18, 24, 29]. In subsequent articles of different authors, these views were considered as decisive in the Lower Precambrian stratigraphy of the Batomga megablock, being accepted as a basis for the development of the current stratigraphic scales and for defining the stages of magmatism [11, 12, etc.].

In 1988–1998, the Batomga inlier and surrounding structures were covered by large-scale mapping and special works, which were accompanied by multichannel airborne gamma spectrometry, geochemical and geophysical surveying, and drilling [11, 12, 38]. The obtained new factual data changed substantially the traditional views on the Early Precambrian geology of this area. For example, discrimination of the Maimakan Formation in the stratotype area on the watershed between the Maimakan and Chumikan rivers was declared to be invalid [3]. In fact, these outcrops represent the Utukachan and Odola formations saturated with intrusive bodies of the Utukachan (metabasites), Dzhagdakan (gneissoid quartz diorites), and Khoyunda (granitoids) complexes, which were erroneously identified with compositionally variable gneisses. The Odola Formation appeared to unite the altered mafic–ultramafic and dioritoid rocks of the Chumikan (Konder) and Dzhagdakan complexes, respectively, which formerly served as a basis for defining the oldest Omnya Complex of rocks metamorphosed to the granulite facies [28]. The gneissoid mafic–ultramafic and dioritoid rocks with magmatic textures were identified by some researchers as amphibolized two-pyroxene and pyroxene crystalline schists and plagiogneisses [18, 28, 29]. The presence of metamorphites of the granulite facies, i.e., rocks of the Omnya Complex in the understanding of Neelov et al. [28], received no confirmation by the results of large-scale geological surveys [11, 38]. According to the Rb–Sr isochron dating, the gneisses of the Utukachan Formation and associated intrusions of Khoyunda granitoids and Dzhagdakan dioritoids were formed 2209–2070 Ma ago [10, 11], which is close to

**Table 1.** K–Ar, Rb–Sr, and U–Pb geochronological data on Lower Precambrian rocks of the Batomga inlier

| Complex, formation | Rock | Sampling site | Analytical method | | | | $^{87}Sr/^{86}Sr$ | Age, Ma |
|---|---|---|---|---|---|---|---|---|
| | | | I | II | III | IV | | |
| Tygymat | Pegmatites and pegmatoid granites (dikes and veins) | Batomga River basin | + | | | | – | 1906 [6–8, 11]; |
| | | | + | | | | – | 1990 [6–8, 11]; |
| | | | + | | | | – | 2100 [6–8, 11] |
| Khoyunda | Plagiogranite, massive | Maimakan–Batomga river interfluve, Odola River basin | + | | | | – | 2210 [6–8, 11] |
| | Plagiogranite, gneissoid (Sample 113) | Chumikan River basin, left tributary of the Maimakan River | | + | | | 0.70194 ± 0.0028 | 2180 ± 140 [11] |
| | Plagiogranite, gneissoid (Sample 114) | Right side of the Maimakan River | | + | | | 0.70272 ± 0.00125 | 1722 ± 382 [11] |
| | Granite, biotite, gneissoid (Sample 115) | Left side of the Maimakan River | | + | | | 0.70150 ± 0.00020 | 2209 ± 99 [11] |
| | Plagiogranite, biotite, gneissoid (Sample B-1/113) | Right side of the lower reaches of the Batomga River | | | + | | – | 2055 ± 7 [26] |
| | Granodiorite, hornblende–biotite, gneissoid (Sample D-09-17) | Left side of the Uchur River | | | | + | – | 2057 ± 13 [14] |
| | Plagiogranite, biotite, gneissoid (Sample D-09-18) | Right side of the Uchur River | | | | + | – | 2053 ± 8 [14] |
| Dzhagdakan | Diorite, gneissoid | Batomga River basin | + | | | | – | 2318 [6–8, 11] |
| | Quartz diorite, biotite–hornblende (Sample 119) | Left side of the Maimakan River | | + | | | 0.70170 ± 0.000150 | 2068 ± 32 [11] |
| | Diorite, amphibole, gneissoid (Sample B-1/12) | Right side of the lower reaches of the Batomga River | | | + | | – | 2062 ± 14 [26]; |
| | | | | | + | | – | 1920 ± 8 [26] |
| Utukachan | Gneiss, garnet–biotite (Sample 112) | Dzhagdakan River basin, left side of the Maimakan River | | + | | | 0.70191 ± 0.0031 | 2176 ± 35 [11] |

The methods used for determining the age of the rocks are designated by Roman numerals: (I) K–Ar on biotite; (II) Rb–Sr isochron; (III) U–Pb on zircons; (IV) U–Pb on zircons, SHRIMP II. Crosses indicate methods used for dating of particular rocks. In the last column, references to published sources (in square brackets).

the K–Ar estimates of the age of the migmatites from the same complexes (Table 1). However, these dates were considered to correspond to the age of the superposed processes [17, 29].

Taking into consideration the recent geological data, the structural position and validity of the Chumikan Complex in the understanding of [17, 28, 29] are cast into significant doubt. "As a matter of fact, this complex unites the rocks of the intricate Chumikan tectonization zone, which comprises spatially juxtaposed chaotically alternating rocks of different ages and different petro- and lithogenetic types" [38]. The Chumikan fault zone (60 × 13 km in size) is characterized by many disjunctive fractures with planes intricately interacting with each other to form a system of different-size longitudinal blocks, sheets, and lenses (Fig. 1). The fold–block–thrust patterns of this zone determined its peculiar "keyboard" structure, wherein the outcrops of tectonized rocks of the "Chumikan Group" are separated by blocks of different rocks of the crystalline basement, which experienced frequently superposed structural–metamorphic transformations [10, 38].

The Sm–Nd model ages (TNd(DM)) are estimated to be 2.1–2.2 Ga for the gneisses of primary sedimentary origin from the Omnya and Batomga sequence, 2.1 Ga for the Chumikan sequence, and 2.0–2.3 Ga for the compositionally diverse granitoids intruding the Omnya and Batomga sequences [19]. They served as a basis for the latter author to conclude that the formation of these granitoids reflects directly the crust-forming events dated to 2.0–2.2 Ga. The authors of [26] estimated the age of the plagiogranites and diorites from the northeastern part of the Batomga inlier (Fig. 1) to be 2055 ± 7 and 2062 ± 14 Ma, respectively (Table 1). In [4, 26], it is also noted that these granitoids experienced gneissization and granulite-facies metamorphism 1920 ± 8 Ma ago, which is evident from the concordant ages of the metamorphic zircon grains from the plagiogranites. In the opinion of [4], these metaintrusions and host intermediate and acid metavolcanics of the Batomga Group form a single primary volcano–plutonic complex of the Batomga granite–greenschist region. Recent studies have revealed "ancient" zircons in Mesozoic intrusions of different composition in this region concordant with U–Pb SHRIMP ages of 2012 ± 23 and 2020 ± 13 Ma for grains from Early Cretaceous granites, 87.4 ± 2.0 Ma (LA ICP-MS, zircon-1), 1060 ± 230, 1781 ± 120, 2268 ± 99, and 2746 ± 120 Ma (LA ICP-MS, zircon-2) for grains from Late Cretaceous nepheline syenites [30]. The dates obtained for the xenogenic zircons reflect most likely different structural–metamorphic events: the oldest of them corresponds evidently to the age of the protolith of the old crustal material. The crystalline rocks of the Batomga block are unconformably (with the erosional surface and weathering crusts) overlain by the Upper Paleoproterozoic sedimentary–volcanogenic sequences of the Ulkan Complex (1.77–1.70 Ga old, according to [12, 13]), which in turn give way after a significant hiatus to sedimentary and volcano–sedimentary rocks of the Mesoproterozoic Uyan and Uchur groups [7, 12] (Fig. 1).

## THE GEOLOGICAL POSITION OF BATOMGA GRANITOIDS

In the inlier structure, a significant role belongs to intrusive rocks (Fig. 1) represented by plagiogranites, quartz diorites, granodiorites, and granites [6–8, 11]. Among them, gneissoid plagiogranites and quartz diorites are most widespread. They form massifs of different sizes and many linear bodies. The largest massifs, 50–270 km$^2$ in size, are characterized by irregular outlines more or less consistent with the strike of the plicative textures of the host metamorphic sequences. Smaller bodies extend usually conformably with the directions of the small folds. The contacts between the intrusions and metamorphic rocks are frequently vague and gradual, representing zones of migmatites, and, less commonly, tectonic. The rocks under consideration are characterized by an irregular distribution of dark minerals, mostly medium-grained composition, and variable textures and structures, frequently gneissoid. They are usually banded, knotted, locally with augen structure, and saturated with xenoliths of plagiogneisses and basic rocks oriented conformably with the strike of the host rocks. The authors of [23] categorized these intrusions into three complexes: Khouynda plagiogranites, Dzhagdakan quartz diorites, and Tygymat leucogranites. Some researchers use another name (Sybakh) for the Khoyunda Complex [24, 29]. In the recent time scale of magmatic processes available for the Batomga block, the Dzhagdakan and Khoyunda complexes are correlated with the Tok–Algoma and Drevnestanovoy complexes, respectively, in the western areas of the Dzhugdzhur–Stanovoi granite–greenschist region [11, 17, 2].

The *Khoyunda intrusive complex* is dominated by plagiogranites accompanied by subordinate granites, granodiorites, and quartz diorites. Gneissoid plagiogranites participate in the structure of many massifs (in some of them together with quartz diorites) and also form autonomous bodies [8, 24]. Most plagiogranite bodies enclosed in the metamorphites of the Batomga Group extend consistently with the strike of the structures in the latter. They form many apophyses along the bedding surfaces in the plagiogneisses and crystalline schists, locally forming zones of lit-par-lit migmatization. At the same time, there are also gently crossing contacts in addition to conformable boundaries. Practically all plagiogranite bodies exhibit variably contrasting shadow textures, restites, and skialiths. They themselves are intruded by leucogranites of the Tygymat Complex.

We have studied the mineral composition, petrogeochemical properties, and isotopic age of the gneissoid plagiogranites and granodiorites of the Khoyunda massif intruded into the metamorphic sequences of the Batomga Group. The petrotypical Khoyunda massif 160 km$^2$ in size is located in the western part of the Batomga inlier on the left and right sides of the Uchur River (Fig. 1). The massif structure is heterogeneous: dominant gneissoid plagiogranites are successively replaced toward contact first by banded granodiorites and then by quartz diorites. In the central part of the massif, plagiogranites give way without distinct transition to gneissoid taxitic granites locally with K feldspar porphyroblasts. The characteristic feature of these rocks is the presence of small xenoliths of biotite–amphibole plagiogneisses with vague lenticular shapes.

The plagiogranites (samples D-09-18, X-09-18, X-09-18-1) are leucocratic pinkish gray fine-to-medium-grained, locally inequigranular gneissoid rocks. They are composed (in %) of plagioclase represented by oligoclase nos. 22–28 and rare andesine no. 32 (40–75), quartz (30–50), biotite (3–10), amphibole (0–5), and muscovite (0–3). The granodiorites (samples D-09-17, X-09-17, X-09-17-1) are characterized by elevated contents of biotite and amphibole (up to 20% in sum). Many rock varieties contain microcline (up to 10–15%). Accessory minerals include magnetite, ilmenite, apatite, titanite, rutile, hematite, garnet, rare zircon, perovskite, and tourmaline [6–8]. The texture is hypidiomorphic–granular, blastohypidiomorphic–granular, and blastogranitic. The rocks demonstrate frequently cataclastic textures. The plagioclase forms tabular grains with polysynthetic twin structure being albitized or epidotized. Pelitized K feldspar largely represented by nonlattice microcline is present in the form of both size-variable isomorphic grains and antiperthite ingrowth in the plagioclase. Quartz is represented by xenomorphic grains with wavy extinction locally occurring in the form of micropoikilitic ingrowths. Amphibole is represented by ordinary hornblende, bluish–brownish or dirty green in color. The amphibole is replaced by biotite with the formation of titanite and magnetite. The biotite and amphibole form euhedral crystals or, less commonly, joint lenticular accumulations visible to the naked eye. Muscovite, epidote, and titanite developed after the greenish–brownish biotite.

The Khoyunda massif is intruded by Late Paleoproterozoic granophyric granites of the Ulkan Complex and overlain by the Middle Mesoproterozoic Konder Formation with weathering crusts at the base and Lower Mesoproterozoic Konkula Formation in the north and south, respectively [10, 11, 38].

In the zones of strong tectonization, including primarily in the Chumikan fault zone, the granitoids of the Khoyunda Complex were subjected to intense dynamometamorphism to become microgranular mostly mica–quartz–albite schists locally with relict deformed grains of plagioclase partly replaced by the albite and lenticular augen of granular quartz [3].

The *Dzhagdakan intrusive complex* is represented by gneissoid and massive quartz diorites, granodiorites, and diorites, mostly biotite–amphibole in mineral composition. They form size-variable bodies conformable with the structures of the metamorphic sequences of the Batomga Group [6–8, 38]. The transition between the intrusions and host rocks is extremely gradual, which locally impedes drawing the boundary between them. The intrusive rocks exhibit many schlieren aggregates with the "shadow appearance," which represent relicts of recrystallized metamorphites of the Batomga Group. The largest bodies and massifs are usually well reflected in the magnetic field. The Dzhagdakan massif of sigmoid shapes (300 km$^2$ in size) is petrotypical among them (Fig. 1). It is composed of quartz diorites, gneissoid and massive, locally slightly banded, taxitic, biotite–hornblende, hornblende–biotite, biotite–clinopyroxene–hornblende, grading into diorites and granodiorites or even plagiogranites in some areas [7].

The quartz diorites are characterized by gneissoid to, less commonly, massive structures. Their texture is inequigranular to porphyroid, blastohypidiomorphic–granular, and, locally, blastogranitic. There are also blastocataclastic and blastocement textures. Dark minerals arranged in the form of chains and groups are frequently found enveloping an "augen" of light-colored minerals. Quartz diorites (Sample X-10-1) and granodiorites (Sample X-10-2) consist of plagioclase nos. 30–34 (60–75%), hornblende (5–15%), biotite (5–10%), quartz (5–15%), occasional clinopyroxene (up to 3–5%), and microcline (up to (1–5%). The diorites exhibit higher contents of dark minerals (from 20 to 35%) accompanied by rare quartz (0–5%). Ore and accessory minerals are similar to their varieties in the Khoyunda plagiogranites.

In the opinion of [6–8], the genesis of the gneissoid quartz diorites and plagiogranites is determined by granitization and palingenesis. The presence of sharp contacts between the above-mentioned rocks and metamorphites of the Batomga Group may be explained by heating and partial melting of the substrate due to metamorphism and subsequent local migrations of melts intruded into the gneisses and crystalline schists. Some researchers believe that the emplacement of the granitoids of the Dzhagdakan and Khoyunda complexes was an asynchronous process [17, 23, 24], although, according to [6–8], the relationships between the rocks of these complexes imply their synchronous formation. Such a conclusion is supported also by geochronological data (U–Pb method) on zircons from diorites and plagiogranites [26]. In the opinion of [4], these rocks belong to the single Early Paleoproterozoic granitoid complex of the Batomga inlier. Table 1 presents the chronological

data on the Khoyunda granitoids and host rocks available in earlier articles of other authors [6–8, 11, 26] and originally in [14].

The metamorphites of the Batomga Group and granitoids of the Khoyunda and Dzhagdakan complexes enclose small lenticular and stratiform bodies and isometric–round intrusions of unmetamorphosed gabbro, pyroxenites, and dunites, which were united into the autonomous Levyi Chumikan Complex [23]. In the recent stratigraphic and magmatic scales [11, 12], these rocks are attributed to the Early Paleoproterozoic *Konder dunite–clinopyroxenite–gabbro complex*, the exact age of which is still unknown. The K–Ar, Rb–Sr, and Sm–Nd dates available for the rocks of the petrotypical Konder massif provide mostly Mesoproterozoic ages, although they are contradictory and frequently inconsistent with the geological relationships. The presence of rounded grains of chromite and clastogenic platinum in the terrigenous rocks of the Mesoproterozoic Konder Formation near the Konder massif is undoubted [11]. It is established that the Konder Formation in the Dagil and Omnya river valleys rests upon the weathering crust of pyroxenites–peridotites of the Konder (Levyi Chumikan) Complex. The K–Ar ages of the glauconites from the sandstones of the Konder Formation in the Konder and Bol'shoi Aim river valleys are estimated to be 1150, 1170, and 1200 Ma [6, 7, 11, 31]. The Rb–Sr isochron age of the subalkaline leucogranites intruding the ultramafic rocks of the massif is 1580 ± 20 Ma [11]. According to [1], the bimodal distribution of U–Pb ages obtained for the "old" zircons from the dunites of the Konder massif (T1 = 2473 ± 21 and T2 = 1885 ± 53 Ma; SHRIMP-II, Center of isotopic investigations of VSEGEI, 14 grains) indicates a most likely Paleoproterozoic age of the protolith of the crust (2.47 Ga) and ultramafics of the Konder massif (1.89 Ga).

The leucocratic granites of the *Tygymat Complex* form several small massifs and a system of small fissure-type massifs in the northern part of the Batomga inlier (Fig. 1) [6, 7, 11]. The small leucogranite bodies are usually oriented discordantly relative to the strike of the host sequences of the Batomga Group. The composition of the leucocratic granites is as follows: microcline–perthite (25–40%), quartz (25–40%), plagioclase nos. 16–24 (25–35%), muscovite (2–5%), biotite (0–4%), accessory minerals (garnet, apatite, zircon, monazite, magnetite). The K–Ar age of the biotites from the rocks of the complex in question is estimated to range from 1.9 to 2.0 Ga [6, 7]. An important role in the formation of the granites of this complex belongs to K-metasomatism, which is evident from the microclinization both of the granitoids and the host rocks [7].

## ANALYTICAL METHODS

The major element contents in the granitoids of the Khyunda Complex were measured by the X-ray fluorescence method and the concentrations of trace elements were estimated by the ICP-MS method. In the latter case, the relative error of the measurements was 5–10%. The samples were analyzed at the Physicochemical Laboratory of ITiG DVO RAN and the Center of Isotopic Investigations of VSEGEI. In addition, the results of silicate analyses available for 11 samples of granitoids stored in the Regional Geological Department Khabarovskgeologiya [11] were also used. The accessory elements in the sampled duplicates of the standard collection of granitoids subjected to silicate analyses were determined in ITiG DVO RAN. The technique of geochemical investigations is described in detail in [15]. Selection and mineralogical investigation of the zircon grains was performed at the Center of Isotopic Investigations of VSEGEI (St. Petersburg) immediately prior to U–Pb isotopic–geochronological measurements.

Accessory zircons were extracted from samples 10–15 kg in weight using the standard technique [19] based on combination of separation by the magnetic field and in heavy liquids. The monofraction of zircon for the isotopic analysis was selected manually under a binocular microscope. The selected crystals were implanted together with zircon standards TEMORA and 91500 (with known U–Th–Pb parameters) into epoxy resin and polished approximately to half of their thickness. The morphology and inner structure of the zircon crystals were studied in transmitted and reflected light. The inner structure of the zircons was also examined using cathode luminescence images. The isotopic dating of the zircons was carried out by microprobe analysis on a raster CamScan MX 2500 electron microscope. The local U–Pb dating of the zircons was conducted on a precision high-resolution secondary-ion microprobe SHRIMP II in accordance with the standard technique [55]. The diameter and depth of the sampling crater were 30 and 3–4 μm, respectively, and the intensity of the primary bunch of molecular negatively charged oxygen ions was 3–4 ηA. The analytical data were processed using the SOUID program [4]. The U–Pb ratios were normalized at the value of 0.0668 assigned to the TEMORA standard of zircon, which corresponds to age of 416.75 Ma [39]. The errors of single analyses (ratios and ages) are given at the 1 σ level and the errors of the calculated concordant ages and intersects with concordia, at 2 σ. The plots with concordia were compiled using the ISOPLOT/EX program [45].

## PETROGEOCHEMICAL PROPERTIES AND GEODYNAMIC TYPIZATION OF GRANITOIDS

Tables 2 and 3 and Figures 2–5 present the data on the chemical composition of the granitoids from the Khoyunda Complex and the distribution of major and trace elements in them. The analyzed rocks are represented by granodiorites and plagiogranites (Table 2)

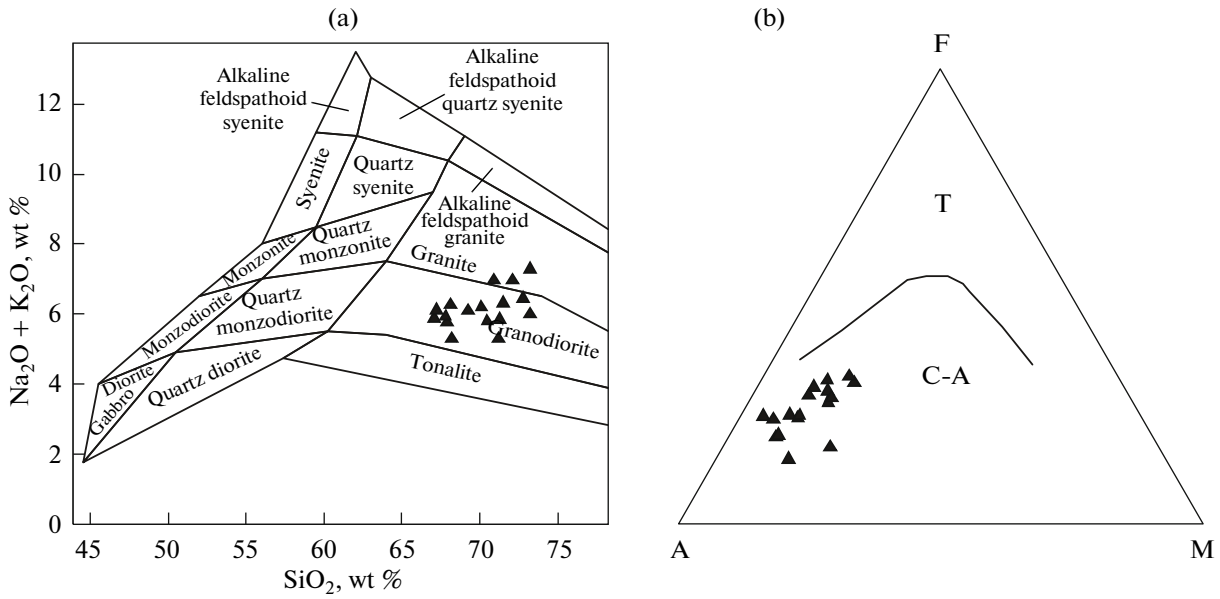


**Fig. 2.** Petrochemical classification diagrams for granitoids of the Khoyunda Complex.
(a) $(Na_2O + K_2O)$–$SiO_2$ [22] diagram; (b) AFM diagram; (T and C-A) fields of tholeiitic and calc-alkaline series, respectively.

with average contents of $SiO_2$ and alkalis of 70.14 ± 2.13 and 6.14 ± 0.54 % (maximum 7.28%), respectively; by these parameters, they fall into the field of low-alkaline granitoids [22]. The data points of their composition are located the fields of granodiorites and diorites in the $(Na_2O + K_2O)$–$SiO_2$ diagram and the fields of calc-alkaline rocks in the AFM diagram (Fig. 2b). As a whole, the Khoyunda granitoids (KHG) are characterized by the following features: prevalence of Fe over Mg; oversaturation with $SiO_2$ and $Al_2O_3$ against the background of moderate and low Mg contents; and enrichment with Ca and N. The agpaitic index in the examined samples varies from 0.50 to 0.66 with the notable prevalence of Na over K. The average composition of these rocks in terms of the concentrations of petrogenic elements is close to that of the granites of the Archean tonalite–trondhjemite–granodiorite (TTG) association [43] except for $K_2O$, the share of which is almost two times lower in the Khoyunda granitoids.

In their chemical composition, practically all of the analyzed granitoids are classified as magnesian (Fig. 3a), high-alumina to, less commonly, meta-aluminous varieties (Fig. 3c) in the calc-alkaline series (Figs. 2b, 3d). In the $(Na_2O + K_2O - CaO)$–$SiO_2$ diagram, the data points of their composition fall into the fields of rocks of the calcic (14 samples) and calc-alkaline (3 samples) series. Such a combination of features of the Khoyunda granitoids gives reason to relate their formation to the settings of island arcs or Cordillera-type volcanic belts, in accordance with the geochemical classification [42]. As follows from Table 2, the Khoyunda granitoids are oversaturated with alumina. For more exact and illustrative characteristic of the Al, alkalis, and Ca balance, we use the modified (Al–K–Na–2Ca) – (Fe + Mg + T) classification diagram [52], which was initially proposed in [41] for discrimination of granitoids into plumasite and aluminous varieties. In this diagram, the data points of the compositions of Khoyunda granites occupy a spacious area from high-plumasite to medium- and low-plumasite to meta-aluminous varieties, which implies the combined composition of the substrate during granitoid melting.

The concentration of transitional coherent elements (Ni, Co, Cr, V) in the Khoyunda granitoids is highly variable, although similar to their contents in the granites of the Archean tonalite–trondhjemite–granodiorite association [43]. However, the Cr concentration in the rocks under consideration is 2.5 times higher as compared with that in the TTG granites. The sum TR (REE) content of TR elements ranges from 48.2 to 88.6 ppm (Table 3), which is more than two times lower than in the granites of the TTG association.

The spidergram in Fig. 4a plotted for the Khoyunda granitoids exhibits distinctly low TR concentrations, low degree of fractionation between their light (L) and heavy (H) varieties ($(La/Yb)_N$, from 17.5 to 35.0), and relatively gentle slope in the plot of the distribution between medium and heavy TR ($(La/Yb)_N$, from 1.99 to 3.24) (Table 3). In the $(La/Yb)_N$–Yb diagram [43], the data points of the compositions of the examined granitoids are located in the field of Early Precambrian rocks of the TTG association. In addition, the TR distribution spectra in

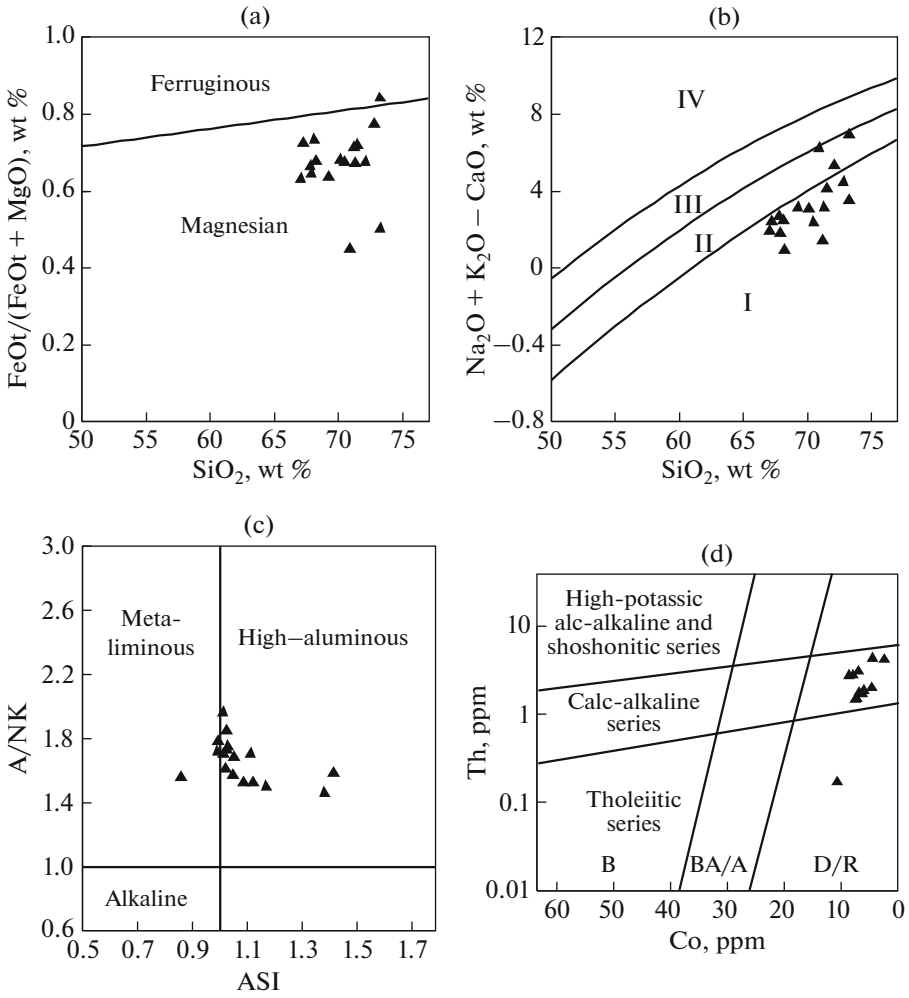


**Fig. 3.** Classification diagrams for granitoids of the Khoyunda Complex.
(a) FeOt/FeOt = MgO diagram [42]; (b) ($Na_2O + K_2O - CaO$)–$SiO_2$ diagram [42]. Fields: calcic (I), calc-alkaline (II), alkaline–calcic (III), and alkaline (IV) series; (c) A/NK = $Al_2O_3/Na_2O + K_2O$ (mol.), ASI = $Al_2O_3/CaO + Na_2O + K_2O$ (mol.); Th – Co diagram [48]. Feld of rocks: (B) basalt, (BA/A) basaltic andesite and andesite, (D/R) dacite–rhyolite.

the analyzed granitoids are characterized by the lack of a negative Eu anomaly (Eu/Eu* = 0.924 ± 0.186; Fig. 4a, Table 3). which may be indicative of the absence of plagioclase in the slightly differentiated source (magmatic chamber), which released material rather quickly [36]. Another peculiar feature of the Khoyunda granitoids is a significant prevalence of light TR (LREE) over heavy TR (HREE): (L/H varies from 13.89 to 16.47 (Table 3) versus 9.54 for the upper continental crust [36] and La/Yb ranges from 17.5 to 35.0). This provides grounds to assume that the granitoids originated from the melted lower continental crust with substantially basic composition, which was to a significant extent depleted.

The mutielement spectra of the analyzed Khoyunda granitoids normalized to the primitive mantle [47] (Fig. 4b) demonstrate the following features: (1) fractionation on account of trace elements; (2) distinct negative trend toward heavy elements and almost mantle concentrations of Ti, Dy, Yb, and Lu. The negative Nb, Ti, Zr, Pr, P and positive Rb, Ba, U, Pb, and Sr anomalies in the same diagram (Fig. 4b) may indicate granitoid melting from a source related to a variable extent to subduction and characterized by mantle signatures [47]. As a whole, the Khoyunda granitoids demonstrate similarity with their counterparts from subduction settings differing from the most widespread varieties in lower HREE concentrations [25, 49]. By several geochemical parameters (Table 3), they are close to the rocks of the back-arc basins, which originated with the contribution both of the depleted upper mantle and enriched plume components [36]. At the same time, the Khoyunda granioids demonstrate similarity with the granitogneisses of the Fedorovka island arc (2003–2013 Ma, U–Pb method, zircon) in the eastern part of the West Aldan megablock [3].

The spidergram in Figure 4 presents multielement spectra for the Khoyunda granitoids normalized to the lower crust [53], which demonstrate their distinct similarity: a practically flat area from K to Yb with values close to 1. In their $^{87}Sr/^{86}Sr$ values of 0.7015 to 0.7027 (Table 1), the Khoyunda granitoids fall into the field of Sr isotopic compositions of the lower continental crust [5, 25]. The substantial accumulation of radioactive Rb, U, and Th (Fig. 4c) is most likely explained by heating and partial melting of the basaltic crust by the ascending plume (U, Th, and Rb in Fig. 4b) [4, 36].

The distribution spectra of REE and other trace elements normalized to chondrite (Fig. 4a) and primitive mantle (Fig. 4b) indicate unanimously that in the situation with Khoyunda granitoids we are dealing with granites of the I- and M-types, not the A-type (Figs. 5a, 5b), formed in the subduction-related settings (LILE enrichment, HFSE depletion, Ta–Nb minimum [5, 36]). In the Pearce discrimination diagram, the Khoyunda granitoids fall into the field of granitoids of volcanic arcs (Fig. 5c), while according to the classification in [54], they belong to the granites of the I- and M-types. The enrichment with Ca and Na, the admixture of lithophile elements, and the low Rb/Sr (0.005–0.025, Table 3) and $^{87}Sr/^{85}Sr$ (Table 1) values give reason to conclude that the examined rocks belong to M-type granites related to island arc volcanism [5]. They are characterized by lower concentrations of trace elements, K, Ti, and Fe (Tables 2, 3) as compared with granites of the I- and S-types [25]. In the Harris diagram (Fig. 5d), the examined rocks fall into the fields of granitoids formed in the late- and postcollisional (6 samples), island arc (2 samples), syncollisional (2 samples), and intraplate (1 sample) environments, although superposition of different geodynamic settings during magma formation, melt evolution, and metamorphism cannot be ruled out [25].

The observable variations in the concentrations of trace elements, Ba, Sr, and K (Table 2) provide grounds for the assumption that fractionation crystallization played a substantially higher role during the formation of the most differentiated varieties of the granitoids of the complex under consideration. This assumption is supported by the diagram in Figure 5e, which identifies the formation mechanism of the igneous rocks: the data points of the Khoyunda granitoids form a trend reflecting fractionation crystallization [40].

All the cited parameters of the Khoyunda granitoids indicate that they belong to the calc-alkaline series and were formed in the geodynamic settings of the active continental margin of the Nevada type (after [35]). The granitoids of this series are subdivided into two groups: granodiorites confined to the peripheral parts of the massifs and adamellites–granites localized in its central part.

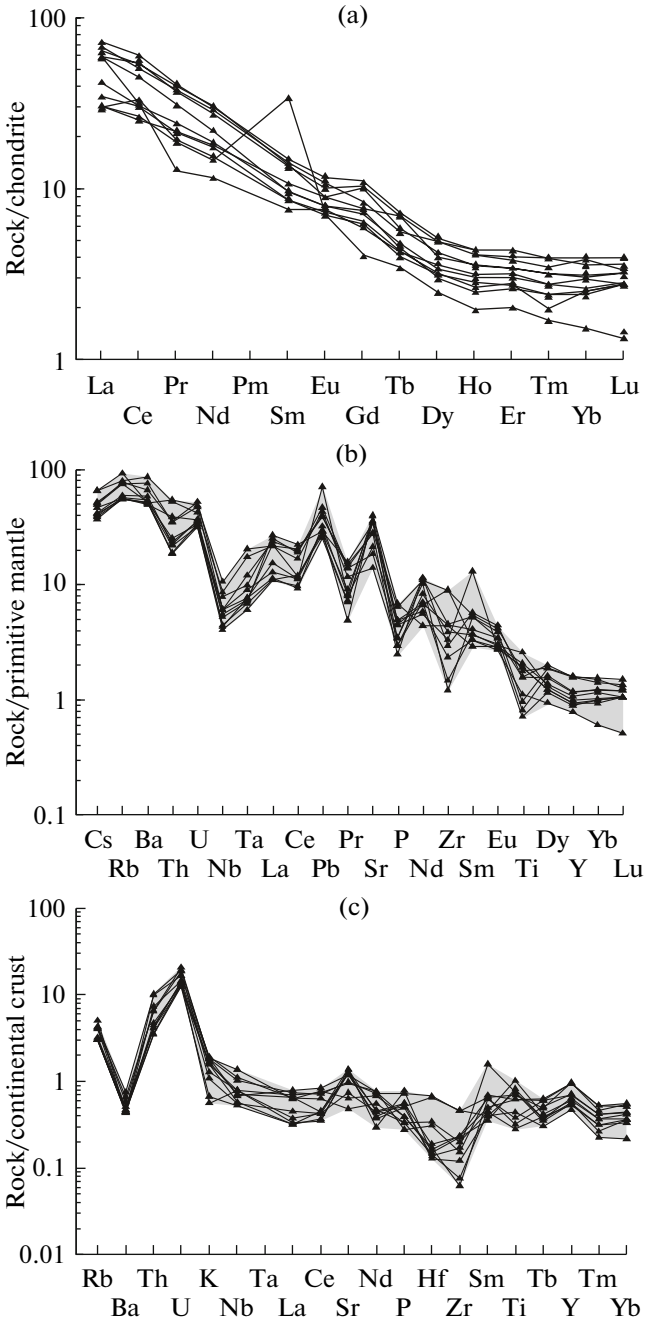


**Fig. 4.** Distribution spectra of REE concentrations normalized to chondrite [51] (a), primitive mantle [4] (b), and lower continental crust [53] (c) in granitoids of the Khoyunda Complex. Gray color designates the field of compositions of Khoyunda granitoids.

## RESULTS OF U–Pb INVESTIGATIONS

The following samples from the Khoyunda Complex were used for geochronological investigations: (1) Sample D-09-17 of fine- to medium-grained gneissoid biotite–amphibole granodiorite (56°53′35″ N, 133°58′08″ E); (2) Sample D-09-18 of fine- to medium-grained gneissoid biotite plagiogranite

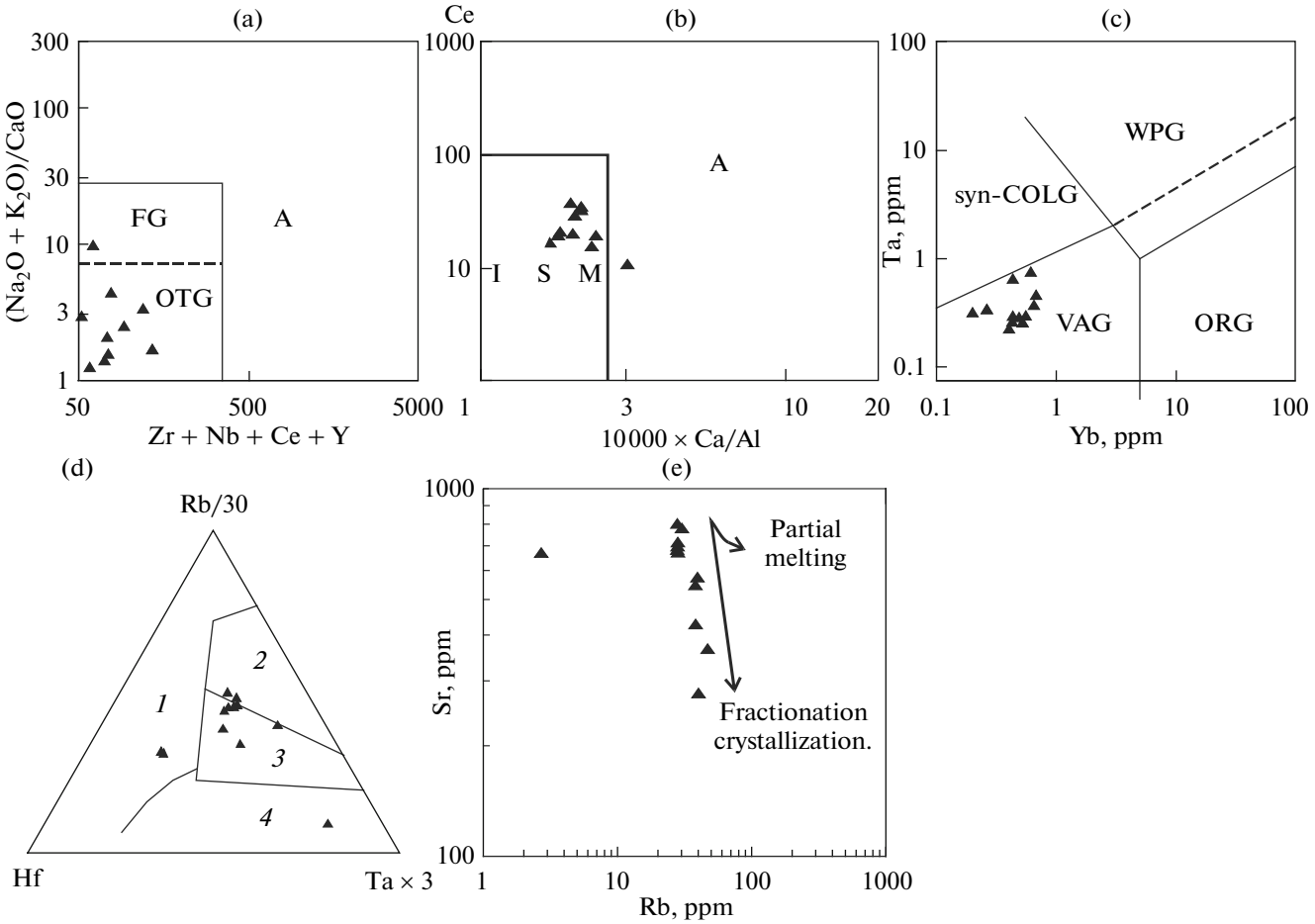


**Fig. 5.** Discrimination diagrams for granitoids from the Khoyunda Complex of the Batomga inlier.
(a, b) ($Na_2O = K_2O/CaO - (Zrb + Ce + Y)$) (a) and Ce – 10000×Ga/Al (b) diagrams [54]. Fields of granitoid compositions: (A) anorogenic, (FG) fractionated type, (OGT) unfractionated type, (M) M-type, (I) I-type, (S) S-type; (c) Ta–Yb diagram [49]. Fields of compositions: (WPG) intraplate, (Sin-COLG) syncollisional, (VAG) volcanic arc, (ORG) mid-oceanic ridges; (d) Rb/30 – Hf – Ta ×3 diagram, after H. Harris [24]. Granitoids: (1) island arc, (2) syncollisional, (3) late- and post-collisional, (4) intraplate; (e) compatible element Sr–incompatible element Rb diagram [40].

(56°56′16″ N, 133°52′20″ E). Table 4 and Figs. 6, 7 present the results of investigations of zircons from the granitoids. Their sampling sites are shown in Figure 1.

Accessory zircon is represented by dull yellow and transparent colorless crystals in Sample D-09-17 and by pinkish brown semitransparent and dull grains in Sample D-09-18, prismatic euhedral and subeuhedral, locally with resorption traces (Sample D-09-17). The grain sizes in Sample D-09-17 vary from 10 to 400 μm, $K_{elong}$ = 1.2–2.6. In Sample D-09-18, these parameters are 100–190 μm and 1.9–3.0, respectively (Fig. 6). No particular differences in the sizes of the zircon grains and their habit in different samples are observable.

The Th/U values for the zircons from Sample D-09-17 are usually 0.30–0.75, which is characteristic of normal magmatic zircons (Th and U concentrations are 21–131 and 60–187 ppm, respectively) (Table 4). In five cases (11.1, 12, 1, 12.2, 1.2, 2.1), the outer rims of zircons yielded Th/U values of 0.2–0.3, which may be indicative of some metasomatic processes. An approximately similar situation is observed for the outer rims of zircon grains from Sample D-09-18, where in three cases (13.1, 15.1, 16.2) the Th/U values varied from 0.14 to 0.23. Thus, the effect of postmagmatic processes in the Khoyunda massif of the Batomga inlier cannot be completely excluded.

In the cathode luminescence images, the zircons usually demonstrate slight luminescence. All the grains exhibit growth phases: distinct fine magmatic zoning in the middle and marginal parts (characteristic of zircons from granites) and coarse zoning patterns in the central parts (characteristic of zircons from gabbro) (Fig. 6). Some grains are characterized by discordance in the orientation of the core and peripheral zones of the crystals. In addition, many zircon crystals demonstrate an outer wider dull rim expanding in their apexes. In some grains, the rim

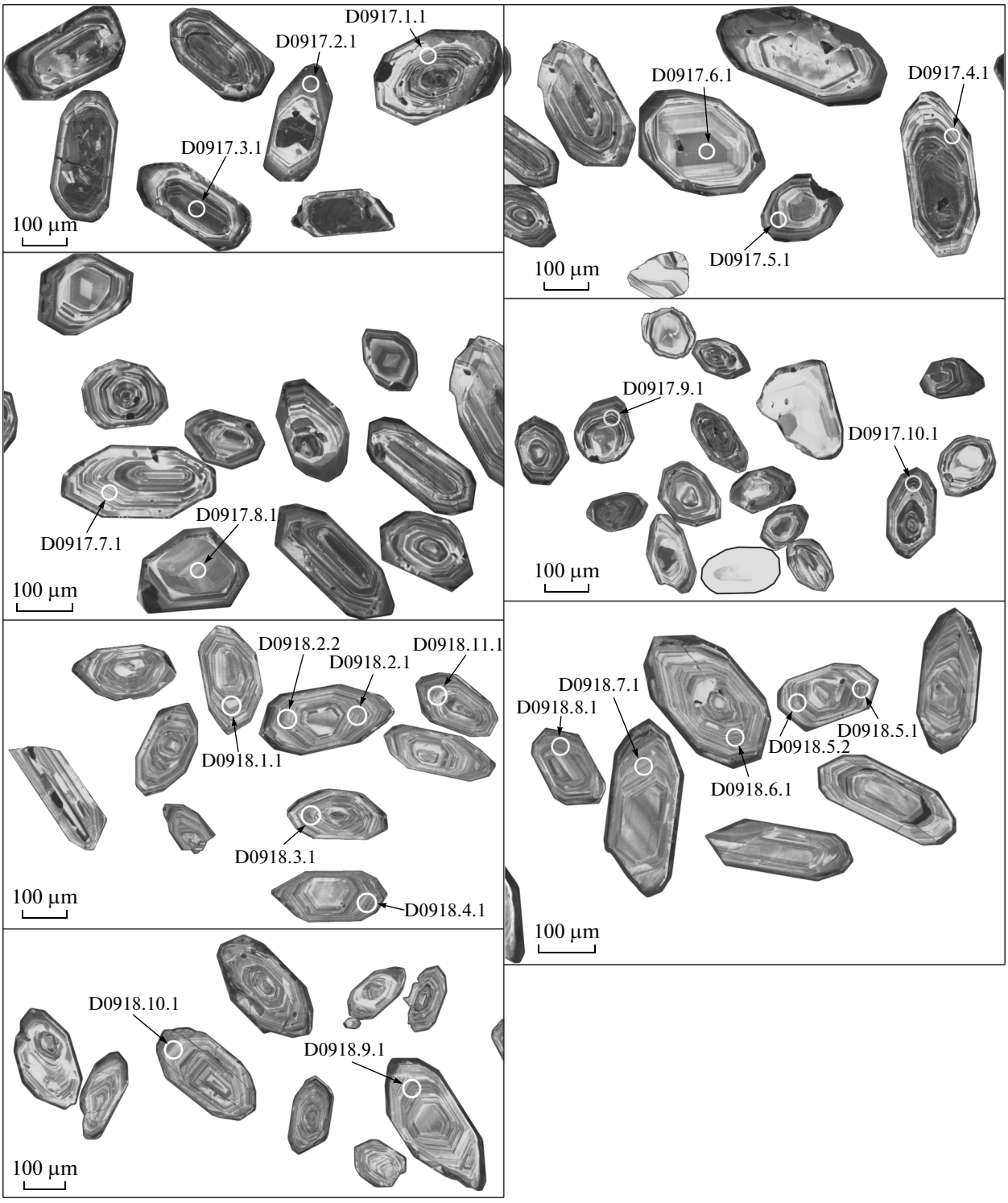


**Fig. 6.** Microimages of zircon crystals (cathode luminescence regime). Numbers of analyzed points as in Table 4.

heals "bights" and "inlets" (Fig. 6) resulting from the resorption of crystals.

For determining the age of the zircons and superposed processes, we have analyzed the central and marginal (with distinct fine zoning) parts of the crystals and their outer rims to increase the number of point measurements from the traditional 10 ([14] Table 1) per sample of granites to 20 for Sample D-09-17 and 23 for Sample D-09-18 (Table 4). The analysis of point determinations revealed that the ages of dif-

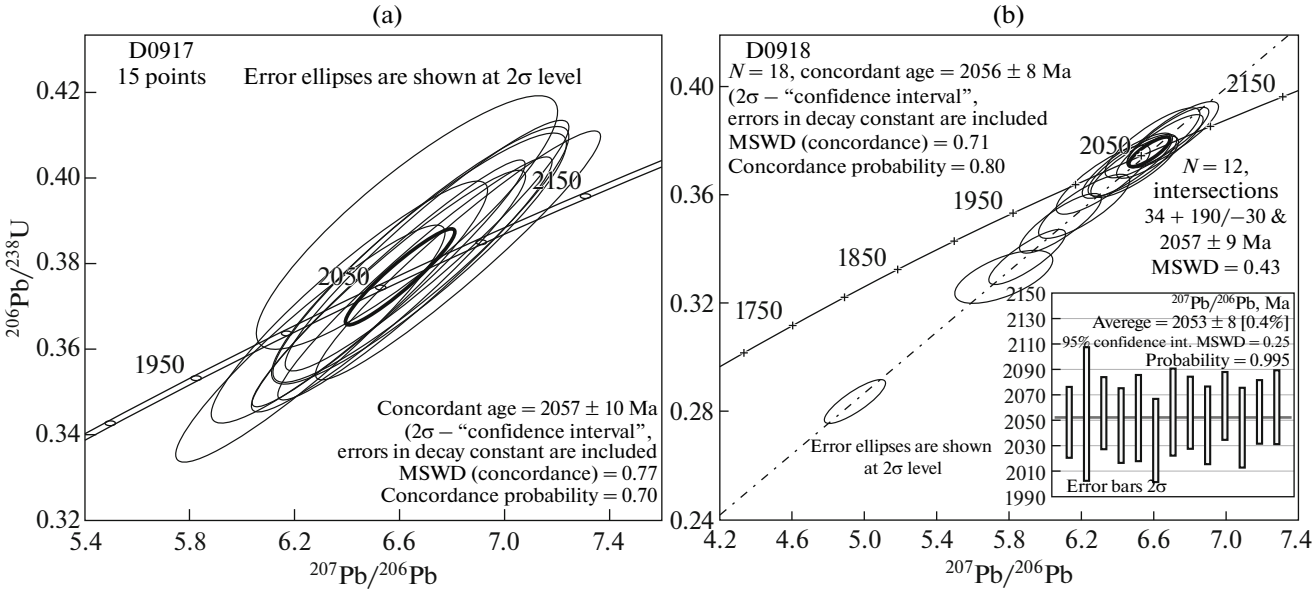


**Fig. 7.** Plots with concordia for zircons from granodiorite (a) and plagiogranite (b). For Sample D0918, the mean $^{207}Pb/^{206}Pb$ age value is weighted only with account for data point errors, 0 from 13 selected; heights of rectangles correspond to the 2σ level.

ferent parts of zircon grains (in both samples, the age of the cores and thin finely zoned rims) are concordant and approximately similar to range from 2030 to 2070 Ma, while most ages of the outer rims are discordant and characterized by lowered values ranging from 1602 to 1991 Ma (Table 4). These discordant values were omitted from calculations. The number of age estimates with discordance <5% which were used for calculations are 15 and 18 for the zircons from samples D-09-17 and D-09-18, respectively (Fig. 7, Table 4). Therefore, the age of granodiorite crystallization is estimated to be 2057 ± 10 Ma for the 15 grains from Sample D-09-17 and 2056 ± 8 Ma for the 18 points in the plagiogranites of Sample D-09-18 (Fig. 7). The discordia compiled for Sample D-09-18 using all points is characterized by the intersect at 2053 ± 8 Ma (Fig. 7). The analysis of the data in Table 4 and Fig. 7 provides grounds to accept average values of 2057 ± 10 Ma (MSWD = 0.77, probability 0.70) and 2056 ± 8 Ma (MSWD = 0.71, probability 0.80), calculated from $^{207}Pb/^{206}Pb$ values for the least "discordant zircons" from Sample D-09-17 (n = 15) and Sample D-09-18 (n = 18), respectively, as representing their age estimates.

## DISCUSSION

The SHRIMP II U–Pb zircon dating of the plagiogranites and granodiorites from the Khoyunda Complex of the Batomga inlier reveals that they are between 2056 ± 8 and 2057 ± 10 Ma old and their formation is related to the Late Paleoproterozoic (late Early Karelian) stage in development of the Batomga granite–greenschist domain. The geological data and the results of geochronological investigations of the granitoids [4, 26] give every reason to conclude that these rocks experienced metamorphic alterations of the amphibolite facies and gneissization 1920 ± 8 Ma ago. The zircons from the granitoids of the Khoyunda [14] and Dzhagdakan [26] complexes are similar in color, morphology, and age to the population of detrital zircons widespread in the sandstones of the Mesoproterozoic Uchur (2025–2065 Ma, U–Pb, [44]) and Kerpyl (2060–1820 Ma, U–Pb, [44]) groups of the southeastern Siberian Platform. For a long period (from 1.65 to .2 Ga [11, 12]), these granitoids of the Batomga inlier served as a main provenance.

It is established that the high-aluminous calc-alkaline Khoyunda granitoids are characterized by moderately fractionated distribution profiles of trace elements, distinct negative trend with respect to heavy elements, and almost mantle Ti, Dy, Yb, and Lu concentrations (Fig 4b). The negative Zr, Ta–Nb, P, and Pr and positive Pb, U, and Sr anomalies indicate presumably granitoid melting from the source related to a variable extent to subduction processes and bearing mantle signatures [47]. As a whole, the Khoyunda granitoids exhibit similarity to their counterparts from subduction settings, however, differing from their most widespread varieties in lower concentrations of heavy TR elements (Y and Yb, 3.29–6.78 and 0.26–0.67 ppm, respectively). The relatively high concentrations of radioactive U, T, and Rb (Figs. 4b, 4c) are most likely determined by heating and partial melting of the lower basaltic crust by magmas of the ascending plume [4, 36]. In the tectonic discrimination diagrams (Figs. 5a, 5b, 5c), the data points of the compositions of the Khoyunda granitoids are located in the field of

**Table 2.** Chemical composition (wt %) of representative granitoids from the Khoyunda Complex

| Component | D-09-17 | D-09-18 | X-09-17 | X-09-18 | X-09-18-1 | X-09-18-2 | 113087 | 11307 | 17172 | 13109 | 11289 | 11469 | 1035 | 13010 | 11388 | 11441 | 11488 |
|---|---|---|---|---|---|---|---|---|---|---|---|---|---|---|---|---|---|
| $SiO_2$ | 68.10 | 72.80 | 67.05 | 72.08 | 73.25 | 70.90 | 73.23 | 71.50 | 70.48 | 71.21 | 69.25 | 68.22 | 70.10 | 67.87 | 67.79 | 67.23 | 71.30 |
| $TiO_2$ | 0.35 | 0.22 | 0.31 | 0.14 | 0.14 | 0.19 | 0.16 | 0.38 | 0.51 | 0.31 | 0.41 | 0.38 | 0.35 | 0.41 | 0.49 | 0.36 | 0.24 |
| $Al_2O_3$ | 15.90 | 14.80 | 16.54 | 15.51 | 15.57 | 16.48 | 13.85 | 14.48 | 15.42 | 13.12 | 14.63 | 16.36 | 15.56 | 15.79 | 14.35 | 16.62 | 15.41 |
| $Fe_2O_3$ | 1.94 | 1.14 | 3.97* | 2.05* | 1.59* | 2.08* | 1.23 | 0.78 | 0.82 | 1.99 | 0.95 | 1.48 | 0.92 | 1.23 | 2.06 | 1.76 | 0.75 |
| FeO | 1.43 | 1.07 | | | | | 0.86 | 1.55 | 1.32 | 1.20 | 1.95 | 1.38 | 1.44 | 1.70 | 1.90 | 1.24 | 0.92 |
| MnO | 0.06 | 0.04 | 0.15 | 0.02 | 0.04 | 0.05 | 0.02 | 0.04 | 0.03 | 0.04 | 0.05 | 0.04 | 0.05 | 0.04 | 0.07 | 0.04 | 0.03 |
| MgO | 1.16 | 0.61 | 2.10 | 0.89 | 1.42 | 2.30 | 0.37 | 0.88 | 0.99 | 1.20 | 1.60 | 1.29 | 1.07 | 1.55 | 1.90 | 1.08 | 0.78 |
| CaO | 3.81 | 1.99 | 3.98 | 1.64 | 0.36 | 0.74 | 2.47 | 2.18 | 3.41 | 3.86 | 2.98 | 4.37 | 3.15 | 3.94 | 3.21 | 3.72 | 2.70 |
| $Na_2O$ | 4.43 | 4.86 | 4.60 | 5.03 | 4.98 | 5.10 | 4.12 | 4.71 | 4.71 | 4.74 | 4.41 | 4.63 | 4.47 | 4.63 | 3.60 | 5.14 | 4.85 |
| $K_2O$ | 1.83 | 1.58 | 1.28 | 1.93 | 2.30 | 1.86 | 1.87 | 1.60 | 1.08 | 0.56 | 1.68 | 0.67 | 1.73 | 1.14 | 2.32 | 0.97 | 0.99 |
| $P_2O_5$ | 0.13 | 0.09 | 0.05 | 0.06 | 0.05 | 0.07 | 0.07 | 0.10 | 0.06 | 0.10 | 0.14 | 0.09 | 0.14 | 0.11 | 0.08 | 0.11 | 0.08 |
| $SO_3$ | | | | | | | 0.10 | 0.10 | 0.10 | 0.10 | 0.10 | 0.10 | 0.00 | 0.10 | 0.10 | 0.10 | 0.10 |
| $CO_2$ | | | | | | | 0.10 | 0.40 | 0.24 | 0.10 | 0.33 | 0.10 | 0.00 | 0.15 | 0.11 | 0.11 | 0.10 |
| $H_2O+$ | | | | | | | 0.53 | 0.79 | 0.49 | 0.38 | 0.71 | 0.67 | 1.10 | 0.66 | 0.85 | 0.52 | 0.66 |
| L.O.I. | 0.69 | 0.77 | 0.11 | 0.56 | 0.29 | 0.18 | 0.54 | 1.06 | 0.64 | 0.43 | 1.03 | 0.57 | 1.19 | 0.76 | 0.86 | 0.40 | 0.73 |
| Sum | 99.83 | 99.97 | 100.14 | 99.91 | 99.99 | 99.95 | 99.52 | 100.55 | 100.30 | 99.34 | 100.22 | 100.35 | 101.27 | 100.08 | 99.69 | 99.40 | 99.64 |
| $Na_2O + K_2O$ | 6.26 | 6.44 | 5.88 | 6.96 | 7.28 | 6.96 | 5.99 | 6.31 | 5.79 | 5.30 | 6.09 | 5.30 | 6.20 | 5.77 | 5.92 | 6.11 | 5.84 |
| $Na_2O/K_2O$ | 2.42 | 3.08 | 3.59 | 2.61 | 2.17 | 2.74 | 2.20 | 2.94 | 4.36 | 8.46 | 2.63 | 6.91 | 2.58 | 4.06 | 1.55 | 5.30 | 4.90 |
| FeOtot | 3.176 | 2.096 | 3.573 | 1.845 | 1.431 | 1.872 | 1.967 | 2.252 | 2.058 | 2.991 | 2.805 | 2.712 | 2.268 | 2.807 | 3.754 | 2.824 | 1.595 |
| FeOt/(FeOt + MgO) | 0.73 | 0.77 | 0.63 | 0.67 | 0.50 | 0.45 | 0.84 | 0.72 | 0.68 | 0.71 | 0.64 | 0.68 | 0.68 | 0.64 | 0.66 | 0.72 | 0.67 |

Analytical methods: X-ray fluorescence spectroscopy (silicate) for samples D-09-17 and D-09-18 (analyst B.A. Timoshenko, Central isotopic center of VSEGEI); X-ray fluorescence spectroscopy for samples X-09-17, X-09-18, and X-09-18-2 (analyst L.M. Il'in, ITiG DVO RAN); silicate for Samples 113087, 11307, 17172, 13109, 11289, 11469, 1035, 13010, 11388, 11441, and 11488 (analysts I.S. Kalabukhova and L.G. Shikhanova, Central laboratory of Khabarovskgeologiya) [11]. *Total Fe in form of $Fe_2O_3$.

**Table 3.** Concentrations of minor elements in granitoids of the Khoyunda Complex (ppm)

| Component | D-09-17 | D-09-18 | X-09-17 | X-09-18 | X-09-18-2 | 113087 | 11307 | 17172 | 13109 | 11289 | 11469 |
|---|---|---|---|---|---|---|---|---|---|---|---|
| Sc | 6.00 | 3.69 | 5.85 | 1.91 | 3.24 | 4.02 | 3.15 | 3.32 | 4.24 | 4.28 | 3.78 |
| V | 49.50 | 28.40 | 44.49 | 11.55 | 18.16 | 46.09 | 34.23 | 33.43 | 39.72 | 38.11 | 37.15 |
| Cr | 54.10 | 64.70 | 91.12 | 85.78 | 84.36 | 89.35 | 68.89 | 62.21 | 84.90 | 89.13 | 56.83 |
| Co | 7.86 | 4.59 | 8.64 | 2.36 | 4.44 | 6.90 | 7.52 | 5.96 | 6.80 | 7.26 | 6.23 |
| Ni | 18.90 | 12.50 | 4.02 | – | 0.89 | 11.74 | 7.18 | 8.13 | 12.69 | 17.66 | 7.85 |
| Rb | 46.50 | 45.10 | 45.22 | 47.48 | 55.65 | 33.31 | 33.20 | 34.25 | 35.46 | 33.15 | 33.76 |
| Sr | 563.00 | 423.00 | 543.97 | 275.27 | 363.78 | 680.00 | 685.00 | 709.00 | 776.00 | 795.00 | 701.00 |
| Y | 6.78 | 3.29 | 6.61 | 3.75 | 6.62 | 4.97 | 3.94 | 4.19 | 4.91 | 4.51 | 3.93 |
| Zr | 92.10 | 93.80 | 30.58 | 40.02 | 12.48 | 46.92 | 24.26 | 15.16 | 46.51 | 45.72 | 34.34 |
| Nb | 5.10 | 3.92 | 3.95 | 5.57 | 6.90 | 3.40 | 2.88 | 2.80 | 3.96 | 3.57 | 2.63 |
| Ta | 0.36 | 0.33 | 0.44 | 0.64 | 0.75 | 0.26 | 0.25 | 0.28 | 0.28 | 0.27 | 0.22 |
| Ba | 438.00 | 344.00 | 498.63 | 568.12 | 334.83 | 327.00 | 337.00 | 357.00 | 385.00 | 343.00 | 336.00 |
| La | 16.30 | 8.23 | 15.29 | 14.00 | 13.90 | 17.35 | 7.05 | 9.91 | 7.28 | 14.34 | 7.01 |
| Ce | 31.50 | 18.70 | 32.81 | 27.85 | 33.99 | 36.88 | 19.98 | 18.59 | 15.37 | 19.44 | 16.14 |
| Pr | 3.54 | 2.00 | 3.75 | 2.93 | 3.48 | 3.95 | 1.81 | 2.28 | 2.05 | 1.23 | 1.77 |
| Nd | 13.50 | 8.16 | 14.19 | 10.24 | 12.57 | 14.02 | 7.21 | 8.69 | 8.44 | 5.43 | 6.87 |
| Sm | 2.18 | 1.32 | 2.29 | 1.47 | 2.07 | 2.11 | 1.32 | 1.49 | 1.64 | 1.16 | 5.26 |
| Eu | 0.63 | 0.41 | 0.67 | 0.46 | 0.59 | 0.52 | 0.43 | 0.45 | 0.52 | 0.44 | 0.42 |
| Gd | 1.73 | 0.83 | 2.32 | 1.53 | 2.12 | 2.08 | 1.31 | 1.49 | 1.58 | 1.23 | 1.28 |
| Tb | 0.21 | 0.13 | 0.27 | 0.17 | 0.26 | 0.22 | 0.16 | 0.18 | 0.26 | 0.16 | 0.15 |
| Dy | 1.25 | 0.62 | 1.32 | 0.76 | 1.24 | 1.07 | 0.81 | 0.87 | 1.02 | 0.91 | 0.81 |
| Ho | 0.23 | 0.11 | 0.25 | 0.14 | 0.23 | 0.20 | 0.16 | 0.17 | 0.20 | 0.18 | 0.15 |
| Er | 0.63 | 0.33 | 0.72 | 0.43 | 0.66 | 0.57 | 0.45 | 0.49 | 0.56 | 0.52 | 0.46 |
| Tm | 0.09 | 0.04 | 0.10 | 0.06 | 0.10 | 0.08 | 0.05 | 0.07 | 0.08 | 0.07 | 0.06 |
| Yb | 0.65 | 0.26 | 0.67 | 0.43 | 0.61 | 0.52 | 0.43 | 0.44 | 0.53 | 0.50 | 0.40 |
| Lu | 0.08 | 0.03 | 0.10 | 0.07 | 0.09 | 0.08 | 0.07 | 0.07 | 0.08 | 0.07 | 0.07 |
| Hf | 2.44 | 2.34 | 1.11 | 1.23 | 0.62 | 0.58 | 0.46 | 0.52 | 0.68 | 0.54 | 0.49 |
| Pb | 6.96 | 10.6 | 5.81 | 6.41 | 5.88 | 4.31 | 3.97 | 4.32 | 4.80 | 4.39 | 3.79 |
| Th | 2.81 | 2.01 | 2.76 | 4.21 | 4.34 | 3.10 | 1.47 | 1.87 | 1.78 | 1.50 | 1.73 |
| U | 1.04 | 0.66 | 0.94 | 0.84 | 0.97 | 0.73 | 0.63 | 0.70 | 0.71 | 0.67 | 0.63 |
| Rb/Sr | 0.08 | 0.11 | 0.08 | 0.17 | 0.15 | 0.05 | 0.04 | 0.05 | 0.04 | 0.04 | 0.05 |
| Pb/Sr | 0.01 | 0.02 | 0.01 | 0.02 | 0.02 | 0.01 | 0.01 | 0.01 | 0.01 | 0.01 | 0.01 |
| Rb/Ba | 0.11 | 0.13 | 0.09 | 0.08 | 0.16 | 0.10 | 0.10 | 0.09 | 0.09 | 0.09 | 0.10 |
| Sr/Nd | 41.70 | 51.84 | 38.33 | 26.88 | 28.94 | 48.50 | 95.01 | 81.58 | 91.94 | 146.41 | 102.03 |
| Eu/Eu* | 0.99 | 1.19 | 0.89 | 0.94 | 0.86 | 0.76 | 0.99 | 0.92 | 0.99 | 1.12 | 0.49 |
| Eu/Sr | 0.01 | 0.01 | 0.01 | 0.01 | 0.01 | 0.01 | 0.01 | 0.01 | 0.01 | 0.01 | 0.01 |
| $Gd_N/Yb_N$ | 2.16 | 2.59 | 2.81 | 2.88 | 2.81 | 3.24 | 2.47 | 2.74 | 2.41 | 1.99 | 2.59 |
| ΣREE | 85.30 | 48.16 | 87.21 | 66.20 | 81.77 | 88.64 | 48.33 | 52.70 | 48.76 | 54.47 | 48.56 |

Samples D-09-17 and D-09-18 are analyzed on the PerkinElmer Elan DRC II ICP-MS System (USA) at the Center of Isotopic Investigations of VSEGEI (analysts E.G. Chervyakova, V.A. Shishlov, and V.L. Kudryashov); other analyses were performed at the Physicochemical Laboratory of ITiG DVO RAN (analysts D.V. Avdeev and A.Yu. Lushnikova). For $La_N/Yb_N$, $La_N/Sm_N$, and $Gd_N/Yb_N$ values, see the text; Eu/Eu* values are normalized to chondrite in accordance with [36]; (ΣREE) sum of rare earth elements except for promethium.

**Table 4.** Analytical data on zircons from granitoids of the Khoyunda Complex

| Analytical point | $^{206}Pb_c$, % | U, ppm | Th, ppm | $^{206}Pb^*$, ppm | $\frac{^{232}Th}{^{238}U}$ | (1) age $\frac{^{206}Pb}{^{238}U}$ Ma | (1) age $\frac{^{207}Pb}{^{206}Pb}$ Ma | Degree of discordance, % | Atomic ratio | | | | | | | | |
|---|---|---|---|---|---|---|---|---|---|---|---|---|---|---|---|---|---|
| | | | | | | | | | (1) $\frac{^{238}U}{^{206}Pb^*}$ | ±, % | (1) $\frac{^{207}Pb^*}{^{206}Pb^*}$ | ±, % | (1) $\frac{^{207}Pb^*}{^{235}U}$ | ±, % | (1) $\frac{^{206}Pb^*}{^{238}U}$ | ±, % | Rho |
| Sample D-09-17 (granodiorite from the Khoyunda massif) | | | | | | | | | | | | | | | | | |
| D0917_14.1 | 2.08 | 364 | 111 | 50.9 | 0.31 | 972 ± 12 | 1983 ± 38 | 55 | 6.14 | 1.33 | 0.12 | 2.12 | 2.73 | 2.50 | 0.16 | 1.33 | 0.53 |
| D0917_12.2 | 8.70 | 468 | 92 | 113.0 | 0.20 | 1602 ± 19 | 2040 ± 67 | 24 | 3.54 | 1.33 | 0.13 | 3.79 | 4.89 | 4.01 | 0.28 | 1.33 | 0.33 |
| D0917_12.1 | 0.66 | 97 | 27 | 27.1 | 0.29 | 1820 ± 26 | 1949 ± 39 | 8 | 3.07 | 1.63 | 0.12 | 2.19 | 5.38 | 2.73 | 0.33 | 1.63 | 0.60 |
| D0917_13.1 | 1.49 | 59 | 13 | 16.8 | 0.23 | 1852 ± 40 | 1947 ± 79 | 6 | 3.01 | 2.49 | 0.12 | 4.41 | 5.48 | 5.07 | 0.33 | 2.49 | 0.49 |
| D0917_13.2 | 0.45 | 125 | 38 | 38.7 | 0.31 | 1978 ± 32 | 2066 ± 45 | 5 | 2.78 | 1.89 | 0.13 | 2.56 | 6.32 | 3.18 | 0.36 | 1.89 | 0.59 |
| D0917_9.1 | 0.16 | 181 | 131 | 56.2 | 0.75 | 1988 ± 54 | 2038 ± 21 | 2 | 2.767 | 3.1 | 0.12 | 1.2 | 6.26 | 3.3 | 0.361 | 3.1 | 0.94 |
| D0917_3.2 | –0.06 | 75 | 22 | 23.3 | 0.31 | 1989 ± 32 | 2059 ± 27 | 4 | 2.77 | 1.87 | 0.13 | 1.51 | 6.34 | 2.40 | 0.36 | 1.87 | 0.78 |
| D0917_14.2 | 0.14 | 105 | 23 | 32.5 | 0.23 | 1991 ± 31 | 2034 ± 36 | 2 | 2.76 | 1.81 | 0.13 | 2.03 | 6.25 | 2.72 | 0.36 | 1.81 | 0.67 |
| D0917_15.1 | 0.07 | 151 | 59 | 46.9 | 0.41 | 1991 ± 25 | 2024 ± 20 | 2 | 2.76 | 1.48 | 0.12 | 1.12 | 6.22 | 1.86 | 0.36 | 1.48 | 0.80 |
| D0917_1.2 | –0.05 | 98 | 23 | 31.0 | 0.24 | 2014 ± 30 | 2058 ± 24 | 3 | 2.73 | 1.73 | 0.13 | 1.36 | 6.43 | 2.20 | 0.37 | 1.73 | 0.79 |
| D0917_8.1 | 0.19 | 109 | 53 | 35 | 0.50 | 2035 ± 54 | 2031 ± 22 | 0 | 2.693 | 3.1 | 0.125 | 1.3 | 6.41 | 3.4 | 0.371 | 3.1 | 0.93 |
| D0917_3.1 | 0.48 | 187 | 92 | 60.4 | 0.51 | 2046 ± 54 | 2061 ± 19 | 1 | 2.675 | 3.1 | 0.127 | 1 | 6.56 | 3.3 | 0.374 | 3.1 | 0.95 |
| D0917_11.1 | –0.02 | 231 | 63 | 74.3 | 0.28 | 2048 ± 23 | 2062 ± 16 | 1 | 2.67 | 1.3 | 0.13 | 0.89 | 6.57 | 1.58 | 0.37 | 1.30 | 0.82 |
| D0917_10.1 | 0.04 | 157 | 96 | 50.6 | 0.63 | 2055 ± 55 | 2052 ± 15 | 0 | 2.663 | 3.1 | 0.127 | 0.85 | 6.56 | 3.3 | 0.375 | 3.1 | 0.96 |
| D0917_4.1 | 0.10 | 162 | 57 | 52.6 | 0.36 | 2060 ± 54 | 2074 ± 16 | 1 | 2.655 | 3.1 | 0.128 | 0.91 | 6.66 | 3.2 | 0.377 | 3.1 | 0.96 |
| D0917_6.1 | 0.26 | 83 | 56 | 27.1 | 0.70 | 2082 ± 56 | 2056 ± 25 | –1 | 2.622 | 3.1 | 0.127 | 1.4 | 6.67 | 3.4 | 0.381 | 3.1 | 0.91 |
| D0917_5.1 | –0.07 | 114 | 45 | 37.5 | 0.40 | 2086 ± 55 | 2091 ± 17 | 0 | 2.618 | 3.1 | 0.129 | 0.97 | 6.82 | 3.3 | 0.382 | 3.1 | 0.95 |
| D0917_7.1 | –0.04 | 60 | 21 | 19.7 | 0.37 | 2087 ± 57 | 2053 ± 23 | –2 | 2.616 | 3.2 | 0.127 | 1.3 | 6.68 | 3.4 | 0.382 | 3.2 | 0.92 |
| D0917_2.1 | 0.10 | 109 | 31 | 36 | 0.30 | 2096 ± 56 | 2053 ± 23 | –2 | 2.616 | 3.2 | 0.127 | 1.1 | 6.7 | 3.3 | 0.384 | 3.1 | 0.95 |
| D0917_1.1 | 0.53 | 108 | 41 | 36.3 | 0.39 | 2121 ± 6 | 2005 ± 30 | –5 | 2.563 | 3.1 | 0.123 | 1.7 | 6.63 | 3.5 | 0.39 | 3.1 | 0.88 |
| Sample D-09-18 (plagiogranite from the Khoyunda massif) | | | | | | | | | | | | | | | | | |
| D0918_15.1 | 0.79 | 236 | 32 | 42.4 | 0.14 | 1225 ± 16 | 2057 ± 35 | 44 | 4.78 | 1.42 | 0.13 | 1.98 | 3.67 | 2.44 | 0.21 | 1.42 | 0.58 |

**Table 4.** (Contd.)

| Analytical point | $^{206}Pb_c$, % | U, ppm | Th, ppm | $^{206}Pb^*$, ppm | $\frac{^{232}Th}{^{238}U}$ | (1) age $\frac{^{206}Pb}{^{238}U}$ Ma | (1) age $\frac{^{207}Pb}{^{206}Pb}$ Ma | Degree of discordance, % | Atomic ratio | | | | | | | | |
|---|---|---|---|---|---|---|---|---|---|---|---|---|---|---|---|---|---|
| | | | | | | | | | (1) $\frac{^{238}U}{^{206}Pb^*}$ | ±, % | (1) $\frac{^{207}Pb^*}{^{206}Pb^*}$ | ±, % | (1) $\frac{^{207}Pb^*}{^{235}U}$ | ±, % | (1) $\frac{^{206}Pb^*}{^{238}U}$ | ±, % | Rho |
| D0918_5.1 | 0.32 | 213 | 95 | 51.9 | 0.46 | 1610 ± 16 | 2049 ± 14 | 24 | 3.52 | 1.16 | 0.13 | 0.78 | 4.95 | 1.40 | 0.28 | 1.16 | 0.83 |
| D0918_12.2 | 0.02 | 256 | 142 | 62.8 | 0.57 | 1618 ± 20 | 2086 ± 18 | 25 | 3.50 | 1.37 | 0.13 | 1.01 | 5.08 | 1.70 | 0.29 | 1.37 | 0.81 |
| D0918_8.1 | 0.19 | 163 | 54 | 46.3 | 0.34 | 1837 ± 19 | 2055 ± 26 | 12 | 3.03 | 1.21 | 0.13 | 1.49 | 5.77 | 1.91 | 0.33 | 1.21 | 0.63 |
| D0918_3.1 | 0.15 | 133 | 65 | 38.6 | 0.51 | 1872 ± 20 | 2056 ± 14 | 10 | 2.97 | 1.24 | 0.13 | 0.80 | 5.90 | 1.48 | 0.34 | 1.24 | 0.84 |
| D0918_9.1 | --- | 115 | 40 | 34.6 | 0.36 | 1932 ± 21 | 2046 ± 15 | 6 | 2.86 | 1.28 | 0.13 | 0.83 | 6.08 | 1.53 | 0.35 | 1.28 | 0.84 |
| D0918_11.1 | 0.03 | 125 | 50 | 37.5 | 0.42 | 1938 ± 27 | 2047 ± 22 | 6 | 2.85 | 1.61 | 0.13 | 1.25 | 6.11 | 2.04 | 0.35 | 1.61 | 0.79 |
| D0918_12.1 | – | 102 | 42 | 31.1 | 0.42 | 1962 ± 23 | 2052 ± 17 | 5 | 2.81 | 1.36 | 0.13 | 0.96 | 6.21 | 1.66 | 0.36 | 1.36 | 0.82 |
| D0918_16.2 | 0.14 | 229 | 51 | 70.0 | 0.23 | 1964 ± 25 | 2075 ± 26 | 6 | 2.81 | 1.51 | 0.13 | 1.47 | 6.30 | 2.11 | 0.36 | 1.51 | 0.71 |
| D0918_14.2 | –0.05 | 104 | 32 | 32.3 | 0.32 | 1989 ± 29 | 2047 ± 31 | 3 | 2.77 | 1.72 | 0.13 | 1.75 | 6.29 | 2.45 | 0.36 | 1.72 | 0.70 |
| D0918_10.1 | 0.00 | 80 | 21 | 25.0 | 0.27 | 2008 ± 24 | 2035 ± 16 | 2 | 2.74 | 1.40 | 0.13 | 0.92 | 6.32 | 1.68 | 0.37 | 1.40 | 0.84 |
| D0918_16.1 | –0.09 | 67 | 19 | 21.2 | 0.30 | 2022 ± 36 | 2045 ± 33 | 1 | 2.71 | 2.10 | 0.13 | 1.87 | 6.41 | 2.81 | 0.37 | 2.10 | 0.75 |
| D0918_2.3 | –0.05 | 104 | 37 | 32.8 | 0.37 | 2023 ± 29 | 2070 ± 23 | 3 | 2.71 | 1.70 | 0.13 | 1.286 | 6.51 | 2.13 | 0.37 | 1.70 | 0.8 |
| D0918_5.2 | 0.32 | 149 | 44 | 47.3 | 0.31 | 2031 ± 22 | 2057 ± 17 | 1 | 2.70 | 1.24 | 0.13 | 0.97 | 6.49 | 1.57 | 0.37 | 1.24 | 0.79 |
| D0918_2.1 | 0.08 | 120 | 39 | 38.2 | 0.33 | 2032 ± 22 | 2056 ± 14 | 1 | 2.70 | 1.27 | 0.13 | 0.80 | 6.49 | 1.50 | 0.37 | 1.27 | 0.84 |
| D0918_7.1 | 0.12 | 104 | 30 | 33.2 | 0.30 | 2033 ± 23 | 2046 ± 15 | 1 | 2.70 | 1.32 | 0.13 | 0.86 | 6.45 | 1.57 | 0.37 | 1.32 | 0.84 |
| D0918_14.1 | 0.44 | 100 | 31 | 31.9 | 0.32 | 2042 ± 32 | 2060 ± 38 | 1 | 2.68 | 1.81 | 0.13 | 2.17 | 6.54 | 2.83 | 0.37 | 1.81 | 0.64 |
| D0918_13.1 | 0.08 | 146 | 22 | 47.5 | 0.15 | 2065 ± 28 | 2113 ± 22 | 3 | 2.65 | 1.56 | 0.13 | 1.23 | 6.83 | 1.98 | 0.38 | 1.26 | 0.86 |
| D0918_4.1 | – | 131 | 39 | 42.6 | 0.31 | 2066 ± 22 | 2062 ± 13 | 0 | 2.65 | 1.26 | 0.13 | 0.76 | 6.63 | 1.47 | 0.38 | 1.26 | 0.86 |
| D0918_9.2 | 0.04 | 86 | 24 | 28.0 | 0.29 | 2067 ± 32 | 2077 ± 28 | 1 | 2.65 | 1.83 | 0.13 | 1.58 | 6.70 | 2.41 | 0.38 | 1.83 | 0.76 |
| D0918_2.2 | 0.00 | 86 | 28 | 28.0 | 0.34 | 2072 ± 24 | 2045 ± 16 | –2 | 2.64 | 1.37 | 0.13 | 0.89 | 6.59 | 1.63 | 0.38 | 1.37 | 0.84 |
| D0918_6.1 | – | 160 | 68 | 52.3 | 0.44 | 2082 ± 22 | 2057 ± 13 | –1 | 2.62 | 1.21 | 0.13 | 0.71 | 6.67 | 1.40 | 0.38 | 1.21 | 0.86 |
| D0918_1.1 | – | 108 | 36 | 35.5 | 0.35 | 2085 ± 23 | 2061 ± 15 | –1 | 2.62 | 1.31 | 0.13 | 0.82 | 6.70 | 1.55 | 0.38 | 1.31 | 0.85 |

All the errors are given at the 1σ level; ($Pb_c$ and Pb*) common and radiogenic lead, respectively. In TEMORA, the calibration error of the standard is 0.31% (1σ). Correction for common lead was performed on the measured $^{204}Pb$. (Rho) coefficient of correlation of the $^{207}Pb/^{235}U$–$^{206}Pb/^{238}U$ values.

volcanic-arc granitoids and correspond to M-type granites.

In their geochemical parameters, the rocks under consideration exhibit similarity to the high-aluminous granodiorites of the Archean TTG association. At the same time, the magmatites of the Khoyunda Complex differ from them in the lower magnesian index (Mg, 0.26–0.52), absence of the Eu anomaly (Fig. 4a), notable prevalence of Na over K, and low concentrations of trace elements. Such geochemical properties imply the formation of primary melts of the plagiogranite–granodiorite group though partial melting of garnet amphibolites [36]. Very low concentrations of heavy trace elements and the negative Ta-Nb anomaly can be due to the presence of restite in hornblende and garnet [36].

The compositionally variable and structurally heterochronous granitoids of the Khoyunda and Dzhagdakan complexes intruding the Paleoproterozoic supracrustal rocks of the Batomga, Omnya, and Chumikan sequences (Batomga Group, after [11, 31]) are characterized by $T_{Nd}(DM)$ = 2.0–2.5 Ga ($T_{Nd}(DM\text{-}2st)$ = 2.2–2.3 Ga), and $\varepsilon_{Nd}$ (1.9) = +0.5 to –3.2 (i.e., close to zero) values [19], which are well consistent with the model of the formation of melts parental for these rocks in the subduction settings through melting of the depleted mantle source with contribution of crustal material [3].

Taking into consideration the Sm–Nd isotopic data available for the Batomga ($T_{Nd}(DM)$ = 2.1 Ga ($T_{Nd}(DM\text{-}2st)$ = 2.2 Ga), Omnya ($T_{Nd}(DM)$ = $T_{Nd}(DM\text{-}2st)$ = 2.2 Ga), and Chumikan ($T_{Nd}(DM)$ = 2.0–2.1 Ga) sequences [19], there is every reason to believe that the formation of the Batomga Group and associated granitoids of the Khoyunda and Dzhagdakan complexes reflects immediately the development of the Early Paleoproterozoic continental crust (2.0–2.2 Ga). The crustal material may have originated either from Late Archean metamorphic or igneous rocks, dated by the U-Pb method (on "old" zircons from younger compositionally different intrusions) to 2.75 Ga (LA ICP-MS, Center of Isotopic Investigations, VSEGEI) [30]) and 2.47 Ga (SHRIMP II, Center of isotopic investigations, VSEGEI) [1]).

The formation of the granites of the Tygymat Complex, spatially juxtaposed with subduction Khoyunda granitoids, was determined by subsequent collisional or accretionary processes.

Calculations of the metamorphism conditions for the rocks of the calc-alkaline series of the Batomga Complex using garnet–amphibole–plagioclase thermobarometry [4] yielded values ranging from 616 to 712°C and from 7.4 to 9.5 kbar. As follows from these calculations, the conditions of culmination of metamorphism and, correspondingly, partial melting with subsequent crystallization of the Khoyunda and Dzhagdakan granitoids correspond in terms of temperature to the transition between amphibolite and granulite facies under elevated pressure values [4, 37]. This means that high-temperature and high-grade metamorphism are subduction-related phenomena, which were realized in the back-arc settings on the active continental margin.

The available data show that the protoliths of gneisses and crystalline schists from the Batomga Complex (Group) were mostly represented by acid, intermediate, and basic volcanics such as rhyolites, dacites, andesites, and basalts belonging, according to [4], to the calc-alkaline and comatiite–tholeiite series. It is highly probable that the metabasites of the Utukachan and Konder intrusive complexes belong to the comatiite–tholeiite series as well. The sections of the Batomga Group also include paragneisses, marbles, and calciphyres. The metavolcanics of the calc-alkaline series exhibit the distribution of minor and trace elements close to that in the Khoyunda granitoids. Like in the latter, they are characterized by distinct negative Ta–Nb, Ti, P and positive Ba and Ta anomalies, moderate fractionation distribution of trace elements ($La_n/Yb_n$ = 14.5–59.2, after [4]), absence of the negative Eu anomaly, and close Nb/Y and Zr/Y values. These features indicate most likely homogeneous parental melts and their belonging to a single volcano–plutonic association. Judging from the geochemical data in [4], the metavolcanics of the Batomga Complex are represented by two groups: (1) rocks of the continuously differentiated island-arc basalt–andesite–dacite–rhyolite series constituting, according to preliminary estimates approximately 70% of the complex; (2) intraplate basalts represented by metabasites compositionally similar to low-Ti traps and varieties compositionally close to basalts of continental rifts. In this connection, it may be concluded that the rocks of the Batomga Group were formed in subduction-related environments [5]. The tectonic position of the intraplate basalts is insufficiently clear. It is conceivable that their formation is related to rifting synchronous with subduction processes and corresponding to initial stages in the development of a back-arc basin and/or superposition of a "hot spot" presumably of the Konder type (1.89 Ga ago).

The Batomga Complex is composed of metavolcanics mostly belonging to the calc-alkaline series, which are identified with island arc products [4]. Their age determined by the R–Sr isochron method on the garnet–biotite gneisses of the basal, Utukachan Formation is estimated to be 2176 ± 35 Ma (Table 1), which is well consistent with the data on the Sm–Nd system [19]. In accordance with these data, the lower age limit of the Batomga Group is placed at 2.2 Ga. The upper age limit is defined by the age of the intruded Khoyunda granitoids, which were emplaced during the culminating stage of metamorphism at the transition between the amphibolite and granulite facies 2.056–2.057 Ga ago.

The Sm–Nd isotopic parameters of the island-arc sedimentary rocks of the Batomga Group and the Khoyunda–Dzhagdakan granitoids of the Batomga inlier [19] are practically identical. In this connection, it is assumed that the granitoids with island-arc properties were formed almost synchronously with the sedimentary–volcanogenic rocks during a single subduction event. The protoliths of the metabasites from the Batomga Complex with intraplate geochemical parameters [4] may have formed under conditions of synchronous and/or subsequent rifting. The protoliths of the calc-alkaline metavolcanics from the same complex represent the age and formation analogs of the subduction Khoyunda–Dzhagdakan granitoids; i.e., the protoliths of the Khoyunda granitoids, with geochemical properties of subduction varieties, were formed against the background of the evolving Batomga island arc.

## CONCLUSIONS

In terms of geology, the presented results give rise to several consequences. It is clear that the views on the tectonic–magmatic evolution of the Batomga inlier of the basement and the granite–greenschist domain as a whole require a cardinal revision. The main tectonic events in this region took place in the Early Paleoproterozoic (late Early Karelian) and defined "oldest" rock complexes cannot be correlated with their "analogs" (petrotypes and stratotypes) in the western areas of the Aldan and Dzhugdzhur–Stanovoi regions. The age estimate of 2.056–2.057 Ga obtained with high accuracy for island-arc granitoids from the petrotypical Khoyunda massif is practically the only proven evidence in favor of Early Karelian subduction events in the southeastern margin of the Siberian Platform.

The volcanic calc-alkaline rocks of the Batomga Group formed in subduction-related settings. The insignificant share of protoliths of metabasalts from this group with "intraplate" geochemical properties may have formed under conditions of synchronous or subsequent rifting and/or "hot spot" superposition. Thus, it is proven that the crystallization of the Khoyunda–Dzhagdakan granitoid bodies and the formation of metavolcanics of the Batomga Group, which reflect the Early Karelian subduction stage in the Paleoproterozoic evolution of the lithosphere of the Batomga block, correspond to the period of 2.2 to 2.0 Ga ago.

The obtained age estimate corresponds to the late Early Karelian, which provides grounds for considering the distribution area of the metamorphosed sedimentary–volcanogenic rocks of the Batomga Group as a stratotype locality for the upper Lower Karelian section of the East Siberia and Far East regions.

## ACKNOWLEDGMENTS

We are grateful to A.B. Kotov and M.A. Mishkin, the reviewers of the manuscript, for their remarks and suggestions, which improved substantially its quality. We thank E.Yu. Didenko and O.M. Men'shikov for their help in preparation of the figures and text. The work was conducted in the framework of the State Assignment of ITiG DVO RAN and Program of Basic Research of DVO RAN ("Far East," project no. 15-I-2-030).

## REFERENCES

1. I. Yu. Badanina and K. N. Malitch, Polychronous age of zircons in the dunites of the Konder massif (Aldan Province, Russia), in *Proceedings of 5th All-Russia Conference on Isotope Geochronology. Geochronological Isotope Systems, Methods of their Study, and Chronology of Geological Processes, Moscow, Russia, 2012* (IGEM, Moscow, 2012), pp. 49–52 [in Russian].
2. E. V. Bibikova, *U-Pb Geochronology of the Early Stages of the Evolution of Ancient Shields* (Nauka, Moscow, 1989) [in Russian].
3. S. D. Velikoslavinskii, A. B. Kotov, E. B. Sal'nikova, V. P. Kovach, and A. M. Larin, "Early Precambrian granite–gneiss complexes in the central Aldan Shield," Petrology **19** (4), 382–398 (2011).
4. G. M. Vovna, M. A. Mishkin, A. M. Lennikov, R. A. Oktyabr'skii, V. F. Polin, Z. G. Badredinov, and T. A. Yasnygina, "Geochemistry and metamorphic parameters of rocks in the Batomga granite–greenstone terrane, Aldan Shield," Geochem. Int. **51** (12), 968–980 (2013).
5. *Geodynamic Reconstructions. Methodical Guide*, Ed. by I.N. Abramovich, A.I. Burde, V.D. Voznesenskii, et al., (Nedra, Leningrad, 1989) [in Russian].
6. *Geological Map of the USSR. 1 : 200000. Aldan Series. Sheet O-XXVIII. Explanatory Note*, Ed. by I.I. Filichev and G.I. Rudakov (Moscow, 1981) [in Russian].
7. *Geological Map of the USSR. 1 : 200 000. Aldan Series. Sheet O-53-XXVII. Explanatory Note*, Ed. by S.E. Loseva (Moscow, 1981) [in Russian].
8. *Geological Map of the USSR. 1 : 200 000. Maiskaya Series. Sheet O-53-XXIX. Explanatory Note*, Ed. by A.L. Stavtsev, V.R. Alekseev, and A.P. Kanaev (Moscow, 1971) [in Russian].
9. V. A. Glebovitsky, V. Ya. Khil'tova, and I. K. Kozakov, "Tectonics of the Siberian Craton: interpretation of geological, geophysical, geochronological, and isotopic geochemical data," Geotectonics *42* (1), 8–20.
10. M. V. Goroshko and V. A. Gur'yanov, " Meso- and Neoproterozoic complexes of the cover in the southeastern Siberian Platform: formation conditions and main tectonic features," Geotectonics *42* (2), 147–161 (2008).
11. *State Geological Map of the Russian Federation. 1 : 1000000 (Thrid Generation). Dal'nevostochnaya Series. Sheet O-53-Nel'kan: Explanatory Note*, Ed. by G.V. Roganov (Kartfabrika VSEGEI, St. Petersburg, 2014) [in Russian].

12. V. A. Gur'yanov, *Geology and Metallogeny of the Ulkan Region (Aldan–Stanovoi Shield)* (Dal'nauka, Vladivostok, 2007) [in Russian].

13. V. A. Gur'yanov, G. V. Roganov, V. N. Zelepugin, M. I. Rozinov, and T. E. Saltykova, "Isotopic–geochronological studies of zircons from the Early Precambrian rocks of the southeastern Aldan–Stanovoy Shield: new results and their geological interpretation," Russ. J. Pac. Geol. **6** (2), 97–113 (2012).

14. V. A. Gur'yanov, V. N. Zelepugin, N. G. Berezhnaya, A. N. Didenko, G. V. Roganov, V. A. Dymovich, A. N. Perestoronin, A. Yu. Peskov, and A. V. Kosynkin, "New age data on the Early Precambrian granitoids of the Khoyunda Complex of the Batomga Uplift (eastern Aldan–Stanovoy shield)," in *Geochronological Isotope Systems, Methods of their Study, and Chronology of Geological Processes. Proceedings of 5th Russian Conference on Isotope Geochronology*, (IGEM RAN, Moscow 2012), pp. 120–122 [in Russian].

15. A. N. Didenko, V. A. Gur'yanov, A. Yu. Peskov, A. N. Perestoronin, D. V. Avdeev, E. V. Bibikova, T. I. Kirnozova, and M. M. Fugzan, "Geochemistry and geochronology of the Proterozoic magmatic rocks of the Ulkan trough: new data," Russ. J. Pac. Geol. **4** (5), 398–417 (2010).

16. V. A. Zlobin, "Petrochemical features of the oldest sequences of the eastern margin of the Siberian Platform," Geol. Geofiz., No. 8, 62–71 (1988).

17. L. P. Karsakov, Extended Abstract of Doctoral Dissertation in Geology and Mienralogy (ITiG DVO RAN, Khabarovsk, 1995).

18. V. I. Kitsul, A. F. Petrov, and A. N. Zedgenizov, "Lithotectonic complexes of the Aldan Shield," in *Main Tectonic Complexes of Siberia* (Nauka, Novosibirsk, 1979), pp. 16–31 [in Russian].

19. A. B. Kotov, Extended Abstract of Doctoral Dissertation in Geology and Mineralogy (IGGD RAN, St. Petersburg, 2003).

20. G. Yu. Lagzdina, E. P. Mironyuk, V. N. Moshkin, et al., "Far East Precambrian metamorphic complexes and scheme of their subdivision," in *Magmatic and Metamorphic Complexes of the Soviet Far East* (Khabarovsk, 1967) [in Russian].

21. V. A. Lubyanovskii, A. F. Petrov, and S. S. Rozhin, "Geology and structure of the Early Precambrian complexes of the Maimakan–Chumikan interfluve (eastern Aldan Shield)," in *Tectonics of the eastern Siberian Platform* (Yakut. Fil. SO AN SSSR, Yakutsk, 1979), pp. 53–61.

22. *Igneous Rocks: Classification, Nomenclature, and Petrography* Ed. by V.I. Gon'shakov (Nauka, Moscow, 1983), Vol. 4, parts 1–2 [in Russian].

23. E. L. Magnushevskii, N. P. Mironyuk, S. G. Petrov, and A. N. Timashkov, "Intrusive complexes of the Uchur River basin," in *Problem of Magmatism, Metamorphism, and Mineralization of Far East. Proceedings of the Far East Regional Petrographic Conference* (Yuzhno-Sakhalinsk, 1988), pp. 28–29 [in Russian].

24. M. V. Martynyuk, S. A. Ryamov, and V. A. Kondrat'eva, *Explanatory Note to the Correlation Scheme of the Magmatic Complexes in the Khabarovsk Krai and Amur District* (DV PGO TsTP, Khabarovsk, 1990) [in Russian].

25. *Method of Geodynamic Analysis during Geological Mapping,* Ed. by N.V. Mezhelovskii, (Nedra, Moscow, 1991) [in Russian].

26. M. A. Mishkin, A. M. Lennikov, T. B. Bayanova, G. M. Vovna, V. G. Sakhno, R. A. Oktyabr'skii, and Z. G. Badredinov, "First results of U–Pb geochronological studies of the Precambrian granitoids of the Batomga Block of the Aldan Shield," Russ. J. Pac. Geol. **4** (3), 223–227 (2010).

27. V. N. Moshkin, "Lower Proterozoic complexes of the Stanovoy and Dzhugdzhur ranges," in *Precambrian of the Eastern USSR* (Gosgeoltekhizdat, Moscow, 1961) [in Russian].

28. A. N. Neelov, V. A. Glebovitskii, V. S. Baikova, G. G. Duk, L. P. Karsakov, R. I. Mil'kevich, I. S. Sedova, and S. I. Turchenko, "Evolution of the metamorphic belts of southeastern East Siberia," in *Metamorphic Belts of the USSR* (Nauka, Leningrad, 1971), pp. 117–144 [in Russian].

29. A. F. Petrov, "Stratigraphy of the Lower Precambrian sediments of the Olekma and Batomga blocks of the Aldan shield," in *Lower Precambrian Stratigraphy of the Far East* (Vladivostok, 1990), pp. 41–49 [in Russian].

30. V. F. Polin, V. A. Glebovitskii, V. V. Mitsuk, V. I. Kiselev, S. Yu. Budnitskii, A. V. Travin, N. G. Rizvanova, N. N. Barinov, N. I. Ekimova, and A. V. Ponomarchuk, "Two-stage formation of the alkaline volcano-plutonic complexes in the Ketkap–Yuna igneous province of the Aldan Shield: new isotopic data," Dokl. Earth Sci. **459** (1), 1322–1327 (2014).

31. *Resolution of 4th Interdisciplinary Regional Stratigraphic Conference on the Precambrian and Phanerozoic of southern Far East and East Transbaikalia* (KhGGP, Khabarovsk, 1994) [in Russian].

32. A. P. Smelov, *Metamorphic Evolution of the Olekma Granite–Greenstone Terrane* (Nauka, Novosibirsk, 1989) [in Russian].

33. A. P. Smelov and V. F. Timofeev, "Terrane analysis and geodynamic model of the North Asian craton in the Early Precambrian," Tikhookean. Geol. **22** (6), 42–54 (2003).

34. A. P. Smelov, E. A. Belousova, A. I. Zaitsev, O. B. Oleinikov, A. D. Pavlushin, and N. A. Oparin, "First data on composition and age of the buried basement of the Aldan anteclise (Siberian Platform): dating of xenogenic zircon from the Manchary kimberlite pipe," Otechestvennaya Geol., No. 5, 68–72 (2013).

35. Tauson, L.V., *Geochemical Types and Mineral Potential of Granitoids* (Nauka, Moscow, 1977).

36. S. R. Taylor and S. M. McLennan, *The Continental Crust: its Composition and Evolution* (Blackwell, London, 1985).

37. V. V. Fed'kin, V. I. Kitsul, and V. I. Berezkin, "Mineral compositions and metamorphic P–T conditions of biotite–garnet gneisses from the Batomga Block," Petrology **4** (2), 192–207 (1996).

38. V. E. Chepygin, "Chumikan Group: problems of distinguishment and dating," in *Geology and Mineral Resources of the Amur Region* (Magellan, Khabarovsk, 1999), pp. 94–97 [in Russian].

39. L. P. Black and S. L. Kamo, et al., "TEMORA I: a new zircon standard for U-Pb geochronology," Chem. Geol. **200**, 155–170 (2003).

40. A. Cocherie, "Systematic use of trace element distribution patterns in log-log diagrams for plutonic suites," Geochim. Cosmochim. Acta **50**, 2517–2522 (1986).

41. F. Debon and P. Le Fort "A chemical–mineralogical classification of common plutonic rocks and associations," Trans. R. Soc. Edinburgh Earth Sci. **73**, 135–149 (1983).

42. B. R. Frost, C. G. Barnes, W. J. Collins, R. J. Arculus, D. J. Ellis, and C. D. Frost, "A geochemical classification for granitic rocks," J. Petrol. **42**, 2033–2048 (2001).

43. A. I. S. Kemp and C. J. Hawkesworth, "Granitic perspectives on the generation and secular evolution of the continental crust," in *Treatise on Geochemistry*, Ed. by H.D. Holland, K.K. Turekian (Elsevier, Amsterdam, 2004), Vol. 3, pp. 349–410.

44. A. K. Khudoley, R. N. Rainbird, R. A. Stern, A. P. Kropachev, L. M. Heaman, A. M. Zanin, V. N. Podkovyrov, V. N. Belova, and V. I. Sukhorukov, "Sedimentary evolution of the Riphean–Vendian basin of southeastern Siberia," Precambrian Res. **111**, 129–163 (2001).

45. K. R. Ludwig, "User's manual for Isoplot/Ex, Version 2.10. A Geochronological toolkit for Microsoft Excel," Berkeley Geochronol. Center Spec. Publ. Berkeley, USA, No. 2, 54 (2000).

46. K. R. Ludwig, "SQUID 1.00, A user's manual," Berkeley Geochronol. Center Spec. Publ. Berkeley, USA, No. 1a, (1999).

47. W. McDonough and S. S. Sun, "The composition of the Earth," Chem. Geol. **120**, 223–253 (1995).

48. E. A. K. Middlemost, "Naming materials in magma/igneous rock system," Earth Sci. Rev. **37**, 215–224 (1994).

49. J. A. Pearce, N. W. Harris, and A. G. Tindle, "Trace element discrimination diagrams for the tectonic interpretation of granitic rocks," J. Petrol. **25**, 956–983 (1984).

50. A. P. Smelov and V. F. Timofeev, "The age of the north Asian Craton basement: an overview," Gondwana Res. **12**, 279–288 (2007).

51. S. S. Sun and W. F. McDonough, "Chemical and isotopic systematics of oceanic basalts: implications for mantle composition and processes," in *Magmatism in Ocean Basins*, Ed. by A.D. Sauders and M. Norry, Geol. Soc. London, Spec. Publ. **42**, 313–345 (1989).

52. C. Villaseca, L. Barbero, and V. Herreros, "A re-examination of the typology of peraluminous granite types in intracontinental orogenic belts," Tranbs. R. Soc. Edinb., Earth Sci. **89**, 113–119 (1998).

53. B. L. Weaver and J. Tarney, "Empirical approach to estimating the continental crust," Nature **310**, 575–577 (1984).

54. J. B. Whalen, K. L. Currie, and B. W. Chappell, "A-type granites: geochemical characteristics, discrimination and petrogenesis," Contrib. Mineral. Petrol. **95**, 407–419 (1987).

55. I. S. Williams, "U-Th-Pb geochronology by ion microprobe," in *Applications of Microanalytical Techniques to Understanding Mineralizing Processes*, Ed. by M.A. McKibben, W.C. Shanks, and W.I. Ridley, Rev. Econ. Geol. **7**, 1–35 (1998).

*Recommended for publishing by A.P. Sorokin*

*Translated by I. Basov*